Evolution, 2024, **XX(XX)**, 1–20
https://doi.org/10.1093/evolut/qpae142
Advance access publication 5 October 2024
Original Article

OXFORD

Evolution and functional implications of stinger shape in ants

Alexandre Casadei-Ferreira[1], Gabriela Procópio Camacho[2], Thomas van de Kamp[3,4], John E. Lattke[5], Rodrigo Machado Feitosa[5], Evan P. Economo[1]

[1]Biodiversity and Biocomplexity Unit, Okinawa Institute of Science and Technology Graduate University, Onna, Okinawa, Japan
[2]Museu de Zoologia da Universidade de São Paulo, São Paulo, São Paulo, Brazil
[3]Institute for Photon Science and Synchrotron Radiation (IPS), Karlsruhe Institute of Technology (KIT), Eggenstein-Leopoldshafen, Germany
[4]Laboratory for Applications of Synchrotron Radiation, Karlsruhe Institute of Technology (KIT), Karlsruhe, Germany
[5]Departamento de Zoologia, Setor de Ciências Biológicas, Universidade Federal do Paraná, Curitiba, Paraná, Brazil

Corresponding author: Biodiversity and Biocomplexity Unit, Okinawa Institute of Science and Technology Graduate University, Onna, Okinawa, Japan.
Email: alexandrefrreira@gmail.com

Abstract

Trait diversification is often driven by underlying performance tradeoffs in the context of different selective pressures. Evolutionary changes in task specialization may influence how species respond to tradeoffs and alter diversification. We conducted this study to investigate the functional morphology, evolutionary history, and tempo and mode of evolution of the Hymenoptera stinger using Ectatomminae ants as a model clade. We hypothesized that a performance tradeoff surface underlies the diversity of stinger morphology and that shifts between predatory and omnivorous diets mediate the diversification dynamics of the trait. Shape variation was characterized by X-ray microtomography, and the correlation between shape and average values of von Mises stress, as a measure of yield failure criteria under loading conditions typical of puncture scenarios, was determined using finite element analysis. We observed that stinger elongation underlies most of the shape variation but found no evidence of biomechanical tradeoffs in the performance characteristics measured. In addition, omnivores have increased phenotypic shifts and accelerated evolution in performance metrics, suggesting the evolution of dietary flexibility releases selection pressure on a specific function, resulting in a greater phenotypic evolutionary rate. These results increase our understanding of the biomechanical basis of stinger shape, indicate that shape diversity is not the outcome of simple biomechanical optimization, and reveal connections between diet and trait diversification.

Keywords: biomechanics, ectatomminae, finite element analysis, 3D geometric morphometrics

Introduction

As different lineages explore novel opportunities geographically and ecologically (Simpson, 1953), they may undergo adaptive changes to capitalize on these opportunities. Nevertheless, it can be challenging to optimize across the variable functional requirements relevant to a single phenotypic trait or a group of traits (Huey & Hertz, 1984). Generalist organisms may perform reasonably well in multiple tasks but may not be finely tuned and specialized for specific roles (Irschick & Higham, 2016). In contrast, specialization in one task often comes at the expense of suboptimal performance in others (Arnold, 1992; Irshick & Higham, 2016), reflecting the frequent tradeoff between functional flexibility and optimization. Although specialists may benefit from monopolizing a specific resource type, they may compete more intensely with other specialists (Paull et al., 2012) than generalists, as the latter can switch to alternative and underutilized resources. Therefore, resource specialists should have lower fitness than generalists if they are forced to switch to another resource to which they are poorly adapted. Tradeoffs may develop for various reasons, such as resource constraints and mechanical limitations imposed by fundamental physical laws. The conflicting mechanical requirements of diverse anatomical structures often result in certain phenotypes that are well adapted for optimal performance under specific conditions and less suitable for others (Irshick & Higham, 2016). The nuanced interplay between adaptability and task-specific optimization emphasizes the nature of evolutionary compromise, molding a diverse array of phenotypic traits.

Despite differences in size, structure, and evolutionary history, all venom delivery systems follow similar principles when exposed to biologically relevant mechanical stress (Bar-on, 2019). Venom systems must tolerate various contact-induced stresses during penetration of the target tegument without failure (Bar-on, 2019; Jansen van Vuuren et al., 2016; van der Meijden & Kleinteich, 2017). Because the mechanical performance of venom injection tools is often fundamental to an organism's fitness, their structural characteristics may be optimized to resist acute deformation or damage, primarily to reduce stress and maximize fracture propagation on the target (Bar-on, 2019; Bhushan, 2018). Hence, we can anticipate common biophysical principles underlying the evolution of such injection systems (Anderson, 2018; Bar-on, 2019).

Received July 3, 2023; revisions received September 22, 2024; accepted October 3, 2024

Associate Editor: Tristan Stayton; Handling Editor: Miriam Zelditch

The venom apparatus of aculeate Hymenoptera (ants, bees, and wasps) is a highly modified and specialized system for the synthesis, storage, and inoculation of toxins derived from the female ovipositor and accessory glands (Robertson, 1968) and probably evolved as an adaptation to a predatory lifestyle (Macalintal & Starr, 1996; O'Neill, 2001; Polidori, 2011; Sharkey et al., 2012). The evolution of a stinger from an ovipositor has resulted in various morphological adaptations, such as shortening and multiple sclerite fusions, especially the distal fusion of ninth gonapophyzes that have produced the base, bulb, valve chamber, and stylet of a stinger (Packer, 2003; Snodgrass, 1933). It is believed that the dependence of some predatory ant species on live arthropods as a food resource selectively promotes the maintenance of a functional piercing stinger as an offensive weapon, whereas acquiring plant material for feeding (e.g., herbivory and omnivory) is coupled with a simplified and less effective stinger (Kugler, 1979). Therefore, active hunting and piercing defense may result in the unique shape of the stinger, ultimately improving its performance. In this study, three-dimensional (3D) landmark-based geometric morphometrics were used to describe the diversity and evolutionary paths of lineages within stinger shape morphospace. The association between stinger shape and mechanical behavior under distinct biologically relevant loading conditions was evaluated using finite element analysis (FEA). Ants were used as a model to explore the evolution and mechanics of piercing stingers, primarily because of their substantial morphological diversity and the remarkable range of distinct ecological and functional roles played by them.

By integrating a reconstructed phylomorphospace with simulated mechanical behavior, we aimed to determine how well the stinger shape may correlate with load-bearing properties and the implications of stinger shape variation for the evolution of ants. We anticipated that most morphological changes in stinger shape would originate from the elongation of its distal portion (i.e., stylet). We hypothesized that elongation and variation in stylet girth affect stress distribution patterns because stresses in puncturing structures tend to concentrate near the tip, which would cause the dissipation of stress toward its reinforced base, thus reducing the average values of stress on the stylet. In this scenario, elongated stingers would have larger areas of high stress on the stylet and may be more prone to lateral deflection than shorter and sturdier stingers. As ants primarily use their stingers during agonistic interactions (e.g., hunting and fighting), we predicted that the stinger shape would predominantly occupy functionally optimal (i.e., lower average values of von Mises stress) regions of the phylomorphospace, thereby avoiding exacerbated stress and minimizing its possibility of higher average values of von Mises stress, exceeding yield failure criteria. We also hypothesized that the stingers of predominantly predatory ants would experience lower total stress than those of omnivorous species. Predatory ants depend on the stinger to subjugate their prey; in this sense, we may find that its shape is optimized for reducing the average values of equivalent stress. Conversely, omnivorous ants, feeding on a diet supplemented with organic matter or other decaying organisms, would have their stinger released from pressures according to their puncture capability. Hence, its shape may vary for performing different functions (e.g., social communication; trail communication in *Megaponera* [Hölldobler et al., 1994]) and may exhibit shapes that are not optimized for the penetration scenarios we are simulating.

In addition to exploring the shape variation and its functional consequences, we analyzed the tempo, mode, and history of trait evolution using comparative methods. We evaluated whether the macroevolutionary dynamics of phenotypic and functional evolution of predatory lineages differ from those of their sister omnivore clades. We predicted that the phenotype and functional traits have undergone adaptive evolution (i.e., shifts in trait values) in response to ecological factors (e.g., feeding habit), in which a stricter diet (e.g., predatory) will cause accelerated diversification of stinger morphology, based on the premise that dietary specialization can increase diversification rates compared with that in taxa with broader diets (Futuyma & Moreno, 1988; Schluter, 2000). Although generalizations are challenging, numerous studies have demonstrated that dietary specialization can accelerate taxonomic diversification rates (Burin et al., 2016; Price et al., 2012; Rojas et al., 2012). In this context, we hypothesized that predatory habits improve morphological evolutionary rates relative to lineages that supplement their diet with diverse material sources (i.e., omnivores).

Material and methods

Specimens

We focused on the subfamily Ectatomminae that comprises 303 described ant species in 12 extant genera (Bolton, 2024) that are primarily solitary active foragers hunting and scavenging for arthropods on soil and vegetation, with some species recognized as seed harvesters (Gómez & Espadaler, 2013; Thomas & Framenau, 2005) and gatherers of sugar-based resources (e.g., extrafloral nectar and honeydew) (Lachaud, 1990; Passos & Leal, 2019; Ribas et al., 2010; Valenzuela-González et al., 1995). Our sampling of extant ectatommines included one stinger (ninth gonapophyzes) from 32 species representing 11 of the 12 valid genera (Table 1) (specimen size ranging from ML: [diagonal length of the mesosoma in profile] ~0.80 to ~4.80 mm). The specimens used in this study were primarily preserved in ethanol, except for *Bazboltonia microps* (Borgmeier) and *Poneracantha rastrata* (Mayr), which were dried and mounted. Of the 32 scanned specimens, 16 were imaged using a microcomputed tomography (micro-CT/µCT) Zeiss Xradia 510 Versa scanner in the Scientific Imaging Section at Okinawa Institute of Science and Technology Graduate University (OIST) following the iodine staining protocol (specimens immersed in I_2E dissolved in 99% EtOH for 24–72 hr) to improve contrast and controlling the source–detector distance for high output resolution, which resulted in voxel sizes between 0.7 and 2.0 µm (Table 1). The remaining 16 specimens were scanned using a parallel polychromatic X-ray beam at the UFO-I station of the Imaging Cluster at the Karlsruhe Institute of Technology (KIT) (Katzke et al., *submitted*), resulting in voxel sizes between 2.44 and 6.11 µm (Table 1).

Phylogeny

A concatenated ultraconserved element Ectatomminae phylogeny based on a phylogenomic maximum likelihood analysis of a 90% complete data set (150 taxa) (see Camacho et al., 2022) was slightly modified to trim terminals that were not represented within the 32 scanned specimens using the GEIGER package v. 2.0.10 (Pennell et al., 2014) in R (R Development Core Team, version 4.2.2, Vienna, Austria). The trimmed phylogeny was used for comparative and functional analyses and is available

Table 1. Specimens (unique identified code, genus, and species names) and model information also contain the variables used for static structural analysis. The bold line (*Bazboltonia microps*) highlights variables for the model used to calculate the nominal force (refer to the "Loading scenario and boundary conditions" subsection of the *Material and methods* section for more details). Total surface area and volume refer to the stinger 3D model.

Specimen code	Genus	Species	Total surface area (mm^2)	Volume (mm^3)	STL faces (*no*)	Voxel size (μm)	Elements (*no*)	Nodes (*no*)	Nominal force (mN)
CASENT0744028	*Acanthoponera*	*mucronata*	0.20	0.00093	514,728	2.44	1,227,308	1,759,320	0.67
CASENT0745451	*Alfaria*	*minuta*	0.06	0.00014	418,722	1.00	1,174,485	1,695,404	0.19
CASENT0745452	*Alfaria*	*simulans*	0.21	0.00091	373,746	1.56	1,125,099	1,630,385	0.66
CASENT0745461	***Bazboltonia***	***microps***	**0.03**	**0.00005**	**223,320**	**1.00**	**1,181,358**	**1,693,154**	**0.10**
CASENT0744575	*Ectatomma*	*brunneum*	0.78	0.00758	538,910	6.11	1,009,368	1,450,887	2.70
CASENT0744611	*Ectatomma*	*permagnum*	0.68	0.00646	306,946	6.11	1,026,633	1,473,914	2.43
CASENT0745288	*Ectatomma*	*ruidum*	0.64	0.00361	349,244	1.40	1,075,041	1,577,007	1.65
CASENT0744573	*Ectatomma*	*tuberculatum*	0.89	0.00887	329,728	6.11	1,021,123	1,468,579	3.00
CASENT0745460	*Gnamptogenys*	*boliviensis*	0.13	0.00037	469,082	0.90	1,100,498	1,601,999	0.36
CASENT0745458	*Gnamptogenys*	*concinna*	1.13	0.01211	433,292	1.83	1,104,408	1,596,134	3.69
CASENT0744149	*Gnamptogenys*	*continua*	0.25	0.00129	336,238	2.44	1,106,184	1,591,489	0.83
CASENT0744355	*Gnamptogenys*	*horni*	0.04	0.00012	290,390	2.44	1,323,688	1,876,799	0.17
CASENT0744060	*Gnamptogenys*	*sulcata*	0.40	0.00304	310,732	2.44	1,129,764	1,620,681	1.47
CASENT0744318	*Heteroponera*	*dolo*	0.13	0.00060	330,144	2.44	1,101,766	1,576,855	0.50
CASENT0744120	*Heteroponera*	*flava*	0.09	0.00034	182,268	2.44	1,130,407	1,611,806	0.34
CASENT0744055	*Heteroponera*	*panamensis*	0.07	0.00023	248,630	2.44	1,083,358	1,545,135	0.26
CASENT0745422	*Holcoponera*	*crenaticeps*	0.07	0.00020	263,380	1.00	1,002,114	1,440,545	0.24
CASENT0745412	*Holcoponera*	*cribrata*	0.05	0.00013	281,912	0.88	1,024,398	1,471,612	0.18
CASENT0744517	*Holcoponera*	*moelleri*	0.11	0.00050	296,076	2.44	1,047,345	1,543,610	0.44
CASENT0744313	*Holcoponera*	*relicta*	0.03	0.00008	429,526	2.44	1,239,734	1,745,838	0.13
CASENT0744358	*Holcoponera*	*striatula*	0.09	0.00036	239,626	2.44	1,152,208	1,638,353	0.35
CASENT0745462	*Poneracantha*	*rastrata*	0.10	0.00028	190,268	1.00	1,120,525	1,613,229	0.30
CASENT0744463	*Poneracantha*	*triangularis*	0.05	0.00014	463,834	2.44	1,281,101	1,822,181	0.19
CASENT0743977	*Rhytidoponera*	*eremita*	0.33	0.00117	224,888	1.30	1,074,729	1,585,364	0.78
CASENT0745453	*Rhytidoponera*	*metallica*	0.30	0.00114	238,438	1.12	1,006,657	1,470,530	0.76
CASENT0745454	*Rhytidoponera*	*victoriae*	0.13	0.00038	347,410	1.10	1,016,897	1,474,002	0.37
CASENT0745411	*Stictoponera*	*fontana*	0.12	0.00043	282,552	1.30	1,105,227	1,581,211	0.40
CASENT0745410	*Stictoponera*	*menadensis*	0.18	0.00069	413,532	1.30	1,191,060	1,688,104	0.55
CASENT0745413	*Stictoponera*	*treta*	0.09	0.00032	435,418	1.10	1,155,880	1,678,016	0.33
CASENT0744307	*Typhlomyrmex*	*major*	0.04	0.00011	400,568	2.44	1,190,892	1,694,104	0.16
CASENT0745414	*Typhlomyrmex*	*pusillus*	0.07	0.00016	376,666	0.70	1,227,308	1,759,320	0.20
CASENT0744414	*Typhlomyrmex*	*reinchespergeri*	0.07	0.000245	361,512	2.44	1,004,248	1,434,976	0.27

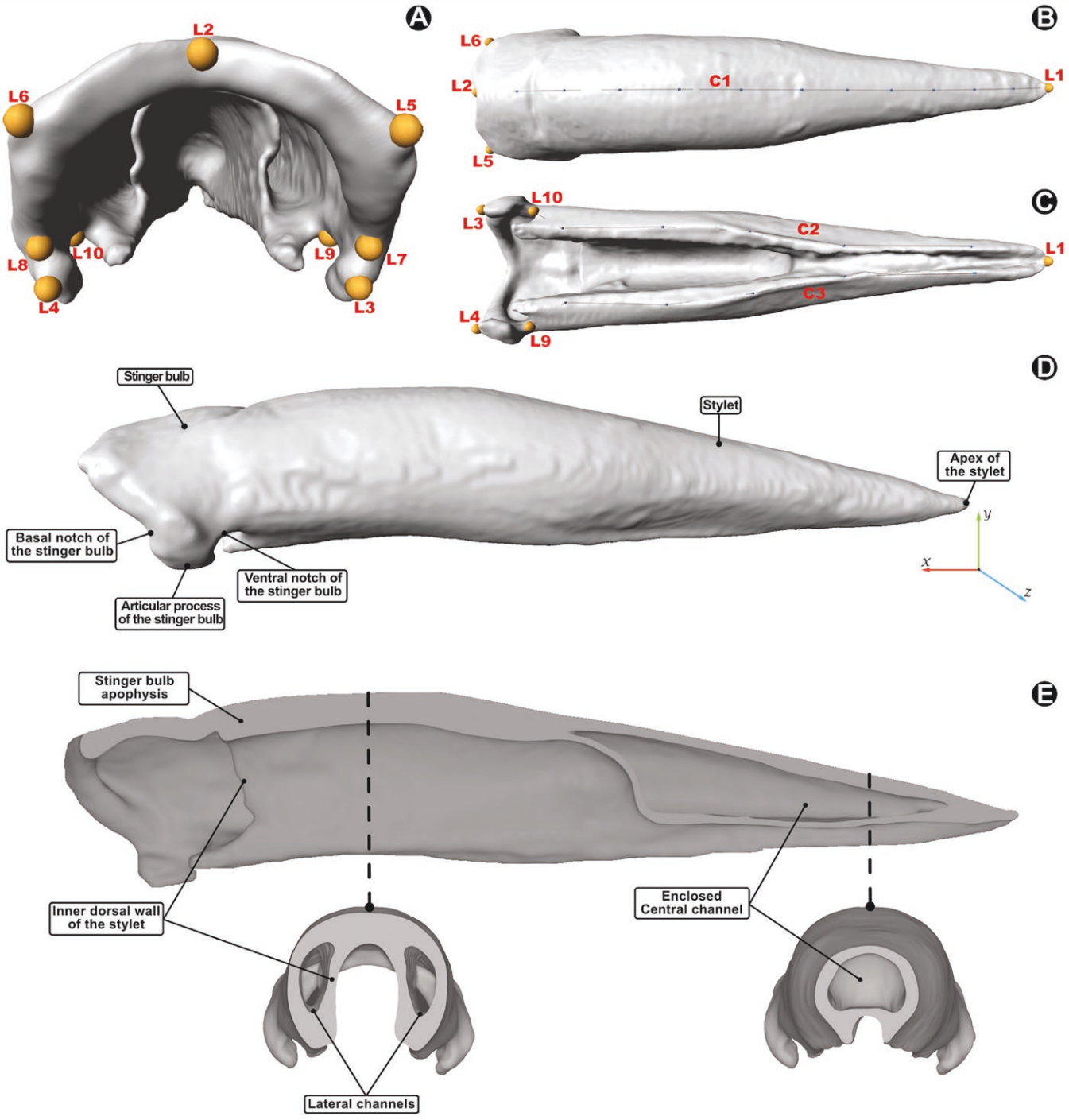

Figure 1. Position of landmarks (L1–10) and semi-landmarks (C1–3) on the stinger along with corresponding terminology. (A) proximal view, (B) dorsal view, (C) ventral view, (D) terminology of different regions of the stinger and the adopted *x-y-z* axis, and (E) longitudinal section of the stinger showing its internal geometry. Dashed lines represent the positions of stinger cross-sections, illustrating the lateral and central channels.

in Supplementary Electronic Material (Supplementary File S1). As some of our analyses depend on a timetree, we derived divergence times by estimating them using the RelTime method (Tamura et al., 2018) in the MEGA11 software (Tamura et al., 2021) using a GTR+Γ5 model of evolution.

3D models

3D reconstructions of the resulting scans were converted into Nrrd ("*nearly raw raster data*"). The Nrrd raw data were processed using 3D Slicer (Fedorv et al., 2012) to segment the stinger. The segmented material was exported as STL ("*standard tessellation language*") and is available in the Supplementary Electronic Material (Supplementary File S2). Blender (Blender, v. 3.1.2, Amsterdam, North Holland, the Netherlands; https://www.blender.org/) was used to (a) reposition all models using the x-axis (refer to Figure 1 for the axis direction) aligned with the stinger's longest principal axis (i.e., defined here as the longest straight line within the stinger that goes from the opening of the venom channel at the stinger bulb to its tip); (b) remove minor surface artifacts; and (c) remesh models applying the modifier "*remesh*" and using the "*smooth*" function, resulting in 3D models with face counting ranging between 182,268 and 538,910 (Table 1). The final STL files were imported into the ANSYS

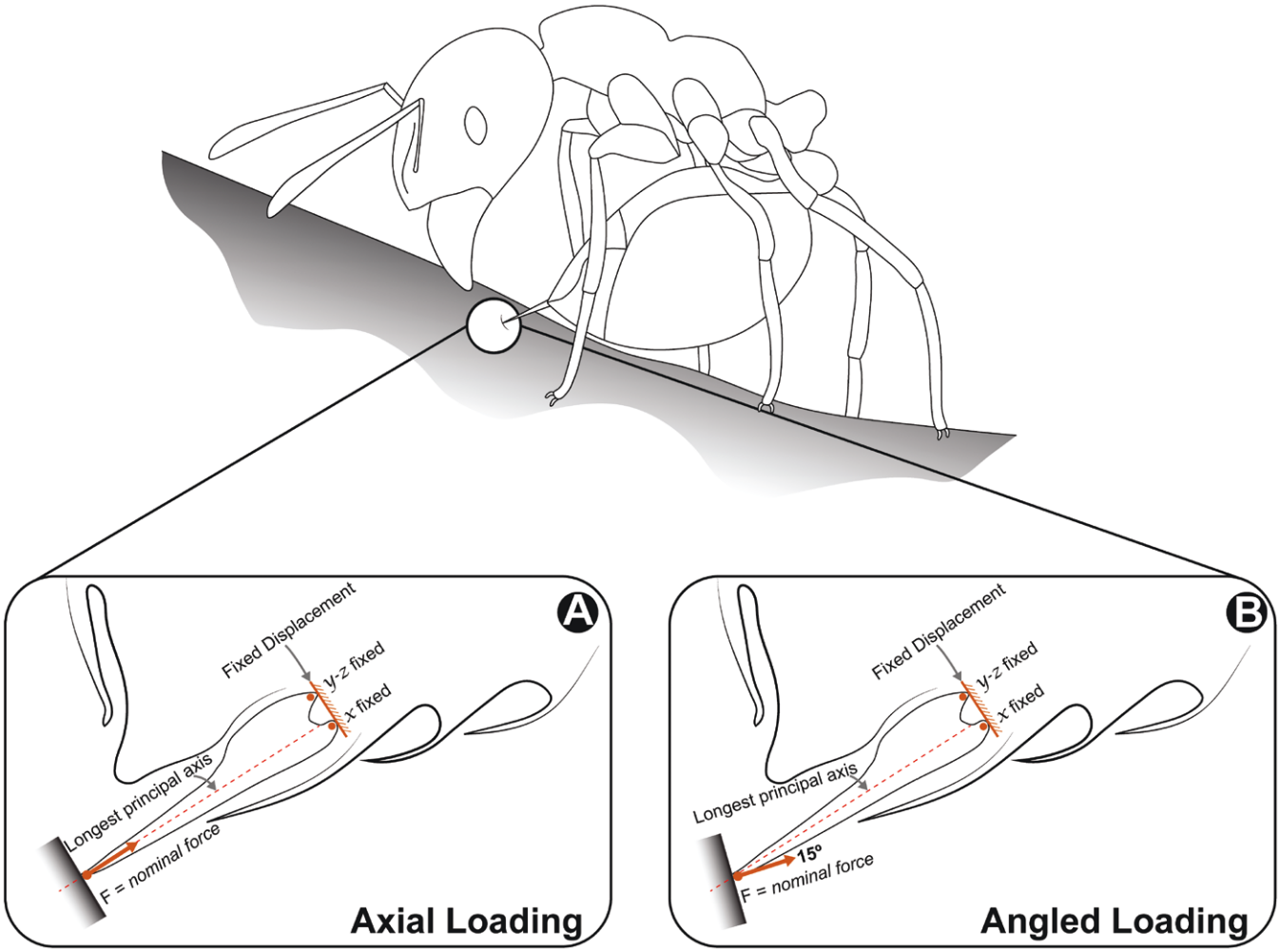

Figure 2. Graphic representation of the stinging process in a generalized hypothetical ant. Loading scenarios tested in the finite element analysis in the puncture loading conditions (A) axial and (B) angled. The orange arrow represents the origin point (circular head) and direction (triangular arrowhead) of the applied force (nominal force); orange dots represent the displacement locations in the *y-z* and *x* directions.

(Asys, Inc., v. 22.1, Canonsburg, PA, USA; http://www.ansys.com/) SpaceClaim module to generate solid models. In SpaceClaim, the STL models were fixed using "*auto fix*," "*shrinkwrap*" tool was used to create watertight, regular faceting models, and "*auto skin*" was performed to generate CAD geometries.

Geometric morphometrics

The stinger shape was quantified using 31 Cartesian coordinates collected from the surface of each model (Figure 1), of which 10 were fixed landmarks, and 21 were sliding semi-landmarks divided into three curves. The landmarks were collected using Stratovan Checkpoint (Stratovan Corporation, v. 2022.07.21.1321, Davis, CA, USA; https://www.stratovan.com/products/checkpoint). The landmarks corresponded to the (L1) apex of the stylet, (L2) midpoint of the proximodorsal margin of the stinger bulb, (L3 and L4) left and right articular process of the stinger bulb, (L5 and L6) left and right proximodorsal process of the stinger bulb, (L7 and L8) left and right basal notch of the stinger bulb, and (L9 and L10) left and right ventral notch of the stinger bulb. The semi-landmark curves corresponded to the (C1) dorsal curvature of the stylet from L4 to L1 (15 sliding semi-landmarks) and (C2 and C3) left and right ventral margins from L9/L10 to L1 (10 sliding semi-landmarks each).

Geometric morphometrics analyses were conducted in R (R Development Core Team, version 4.2.2, Vienna, Austria) using the GEOMORPH package v. 4.0.4 (Baken et al., 2021). Before alignment with Procrustes superimposition, the curves were resampled for evenly spaced sliding semi-landmarks using the "*cursub.interpo*" and "*subsampl.inter*" functions (available in the Supplementary file of Botton-Divet et al., 2016). The landmarks were subject to Procrustes superimposition to remove differences due to scale, translation, and rotation using the "*gpagen*" function. The least squares criterion (Rohlf & Slice, 1990) was used, and the semi-landmarks were allowed to slide between the fixed landmarks. Left- and right-side landmarks and semi-landmarks were averaged to reduce error using the "*bilat.symmetry*" function. The significant components of variation in stinger shape based on Cartesian coordinates were extracted using a principal component (PC) analysis of all specimens to produce a total morphospace using the "*gm.prcomp*" function. Phylomorphospace plots were generated using the PHYTOOLS V. 1.2-0 package (Revell, 2012) through the "*phylomorphospace*" function. A broken-stick model was used to determine the number of PCs that were used in subsequent analyses.

Included angle

We evaluated the stinger tip included angle as a distinct measure of shape. This angle was determined from both lateral and dorsal views of the stinger using scanned volumes, with the mean value used for subsequent analyses. To obtain the included angle for each species, we aligned an isosceles triangle with the stinger, where the equal-length sides matched the lateral margins of the stinger. The base of the triangle was positioned at a set distance (1% of the stylet length) from the stinger tip. The included angle, opposite to the base of the triangle, was then calculated. This method was selected based on its demonstrated efficacy as a predictor of puncture performance (see Crofts et al., 2019).

Finite element analysis

Static structural analysis was conducted using the FEA package ANSYS in a Dell Precision 5820 Tower with 128 GB RAM, Intel Xeon 3.70 GHz, and NVIDIA Quadro RTX 6000 24GB. We used the mechanical properties of the stinger (Young's modulus) derived from previously published data on in vivo nanoindentation of honey bee stingers (Miao et al., 2020). Therefore, we assigned an average Young's modulus value to each model, considering it as an isotropic material (Young's modulus: 8.39 GPa; Poisson's ratio: 0.3). We assumed the material properties to be isotropic, which (a) ensures that the only source of variation in our simulations among different species was the stinger shape, (b) simplifies our analysis, and (c) and allows us to identify relative differences in structural performance (see Fortuny et al., 2012; Gil et al., 2015; Klunk et al., 2021, 2023; Marcé-Nogué et al., 2020; Serrano-Fochs et al., 2015). The stingers were meshed using the ANSYS mesh module with an adaptive mesh of tetrahedral elements (Marcé-Nogué et al., 2015), with an average of approximately 1,500,000 elements (Table 1).

Loading scenario and boundary conditions

All models were fixed in the articular process of the stinger bulb (right and left sides) on the x-axis and the furcula contact area with the proximodorsal process of the stinger bulb (right and left sides) on y- and z-axes (Figures 1D and 2A and B). We assumed that (a) the target is impenetrable and (b) the force driving the stinger is proportional to the size of the stinger. To compare different models and remove the sizing effect, we determined nominal forces (*nominal force* = (*volume of stinger model of target species*/*volume of smallest stinger model*)$^{2/3}$ see Marcé-Nogué, 2020 and Krings et al., 2021 for details) based on a load of 0.1 mN set for the 3D model with the smallest volume (*B. microps*) (Table 1). We used the nominal force because this procedure is a common method for scaling models to a comparable size, effectively addressing scale disparities in the FEA model (Krings et al. 2021; Marcé-Nogué, 2020).

We applied nominal force vectors to test the performance of the stinger, referred to here as the ability of the stinger to present lower average values of von Mises stress, under two distinct puncture loading conditions, viz., (a) axial, where the load was applied to the stinger tip, parallel to its longest principal axis (Figure 2A), and (b) angled, where the load was applied to the stinger tip at an angle (15°) in reference to the x-plane of its longest principal axis (Figure 2B). Because it is not within the scope of this study to analyze the functional differences at different angles of action and considering the absence of precise stinging angle data for ants in the literature, we arbitrarily adopted a 15° angle. However, the selected angle falls within the observed range for bees and wasps, which varies from 6° to 18° (Zhao et al., 2015). We opted to avoid using maximum von Mises stresses as a failure criterion, because our primary focus was on understanding the stress patterns in different stingers. Specifically, our aim was to explore the gradient that reflects the impact of stinger shape on stress field distribution during contact with a target, without the explicit intention of identifying areas prone to failure. Furthermore, we explored the ecological and evolutionary aspects using methods that condense these stress mappings into a single value (e.g., the mesh-weighted arithmetic mean of von Mises stress; see below), which do not require failure criterion approaches.

These puncture loading conditions were considered performance measures due to the expected shift between functional responses from axial compression to bending, which can be caused by a reaction to the curvature in columnar structures (e.g., stinger) (Pohl et al., 2020). In this scenario, straight stingers might tolerate higher axial compression, whereas a curvature in the stylet could potentially reduce stress when loads are applied at an angle to its longest principal axis (Bertram & Biewener, 1988). Moreover, the critical loads at which the stinger becomes unstable were estimated using linear eigenvalue buckling analysis. We used linear eigenvalue buckling as a crucial analysis to evaluate the structural integrity of the stinger under axial loading conditions to understand the specific conditions under which buckling might initiate, thus providing insights into the mechanical behavior and resilience of the stinger. The linear eigenvalue buckling analysis was conducted using ANSYS Workbench on the base static structural solution under axial loading conditions, selecting only the first buckling mode for subsequent analysis.

Phylogenetically informed analysis

The mesh-weighted arithmetic mean of von Mises stress (MWAM; see the Supplementary file of Püschel et al., 2018 for more details) was calculated individually for axial and angled puncture loading conditions after normalizing (by square root) the stress results obtained from the FEA in each model. MWAM was used as a quantitative metric to succinctly summarize the overall strength of the entire stinger model. Biologically, this mesh-weighted average stress value provides insights into the relative biomechanical robustness of the stinger across different taxa and stinging scenarios, offering a comparative understanding of the structural performance under varying mechanical loads.

For calculating the MWAM, we opted to avoid using the top 2% (Marcé-Nogué, 2017) of the highest maximum stress values from each model. This decision was made because the maximum stress values derived from complex finite element models are often influenced by geometric artifacts (Marcé-Nogué, 2016; Marcé-Nogué et al., 2017; Walmsley et al., 2013). The phylogenetic partial least squares (Phylo-PLS) analysis was used to evaluate the covariation between stinger shape (Procrustes shape variables) and functional metrics (puncture loading conditions). The significance of the correlation coefficient (r-PLS) was determined using a randomization test with 1,000 iterations (Adams & Collyer, 2016, 2019; Adams & Felice, 2014; Rohlf & Corti, 2000) using the "*phylo.integration*" function in GEOMORPH. Phylo-PLS analysis was performed by assuming a Brownian motion (BM)

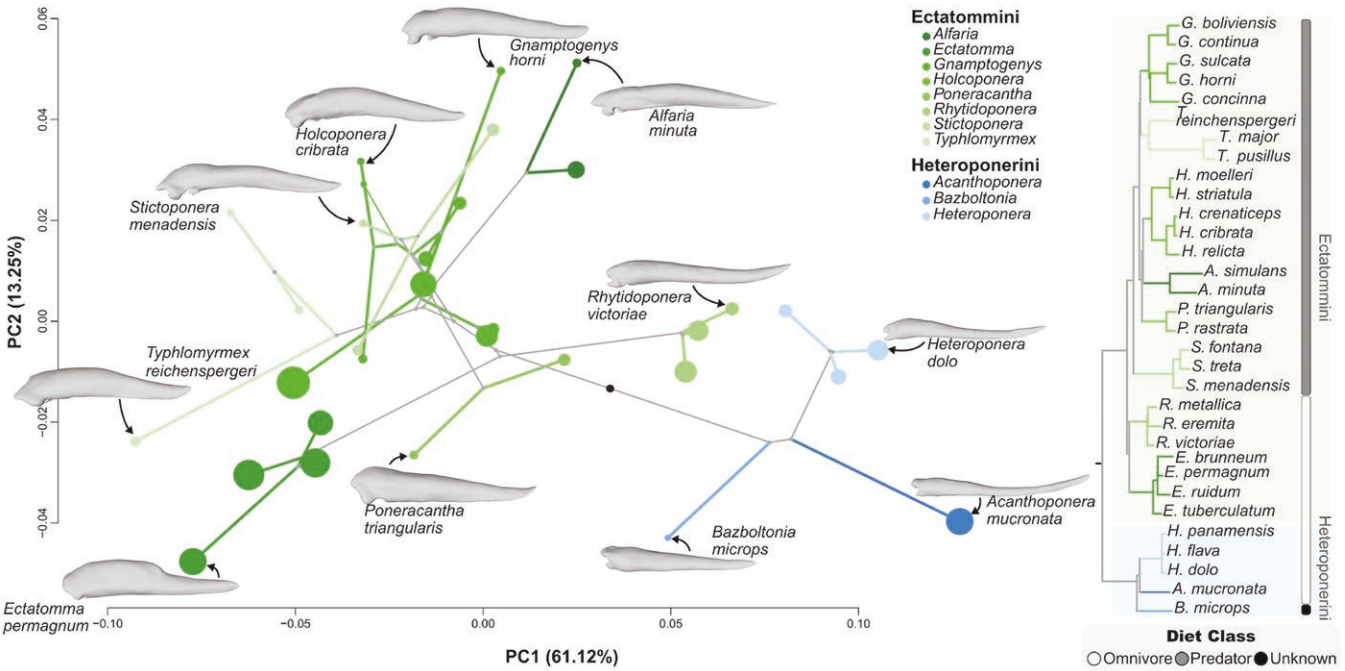

Figure 3. PC1 and PC2 of the stinger phylomorphospace of Ectatominae, with different color groups representing each tribe (Ectatommini and Heteroponerini) and color shades representing different genera. PC1 depicts a clear divergence between the two Ectatomminae tribes and describes the stinger length, slenderness, and curvature, whereas PC2 explains the ventral curvature of the stinger and the length of the articular process of the stinger bulb. Stinger models illustrate the lateral view of the stinger representing all genera and extreme species for each axis. All points are scaled proportionally to the centroid size (i.e., proxy of body size). Simplified phylogenetic tree modified from Camacho et al. (2022). Vertical bars indicate different diet classes (omnivore, predator, and unknown).

model for trait evolution. The strength of the correlation between stinger shape and functional variables was compared between models using *z*-scores under the null hypothesis of a random association of variables (Adams & Collyer, 2016). To visualize shape covariation, the 3D model of *Gnamptogenys continua* (Mayr) (i.e., species closest to the center of the phylomorphospace) was warped on the maximum and minimum shapes of the phylo-PLS using the "*plotRefToTarget*" function in GEOMORPH.

Phylogenetic generalized least squares (PGLS) models (Martins & Hansen, 1996; Revell & Collar, 2009) were used to determine the correlation between the included angle and functional metrics (i.e., axial, angled, and critical buckling loading), accounting for the nonindependence due to phylogenetic relationship. The PGLS models were implemented using the R package NLME v. 3.1-163 (Pinheiro & Bates, 2000; Pinheiro et al., 2023). We performed additional PGLS using a BM model of evolution to assess the relationship between body size (i.e., measured as the distance between the seventh abdominal spiracles) and functional metrics. To account for potential nonlinear relationships, we included a quadratic term for size in the model. Each model was fitted using maximum likelihood, and the significance of predictor terms was assessed using ANOVA.

Macroevolutionary dynamics

A *reversible-jump Markov chain Monte Carlo* (rjMCMC) (Green & Hastie, 2009) approach was used to discern regimes within the phylogenetic comparative data. This method allows the detection of multiple evolutionary regimes across a phylogeny without an a priori hypothesis. rjMCMC was used to fit a multi-regime Ornstein–Uhlenbeck (OU) model to the phylogenetic data to estimate the location, number, and magnitude of shifts in adaptive optima as implemented in the R package BAYOU v 2.2.0 (Uyeda & Harmon, 2014). An a priori distribution was established that accommodated any number of regime shifts per branch, with their probabilities proportional to the respective branch lengths, accessed through 10,000,000 iterations. Subsequently, regimes for all branches in the phylogeny were defined based on the outcomes derived from the BAYOU analyses for each trait under scrutiny (specifically, phenotype represented by PC1, and included angle and performance metrics represented by MWAM and critical buckling load, respectively). Trait histograms aligned with phylogenetic trees were generated, incorporating posterior probabilities from the trait diversification analysis, to visually illustrate variation in the evolutionary regime associated with each tip. We also plotted phylogenetic trees showing the results of the BAYOU rjMCMC analysis, highlighting posterior probabilities ($pp > 0.4$) of regime shifts along the corresponding edges. This approach provides a comprehensive visual representation of the evolutionary dynamics that underpin phenotype and performance metrics.

Lineage-specific variation was evaluated against a standard BM model to ascertain the relative acceleration of evolution within particular lineages compared with a gradual model. Ancestral values were inferred using a multiple variance BM ("mvBM") approach (Smaers & Mongle, 2018; Smaers et al., 2016) as implemented in the EVOMAP v. 0.0.0.9 package (Smaers & Mongle, 2018). Finally, a distance-based method (Q-mode) assuming a standard BM model of evolution with 10,000 random permutations (Adams, 2014; Adams & Collyer, 2018; Baken et al., 2021; Denton & Adams, 2015) was used to discern differences in rate among phenotype

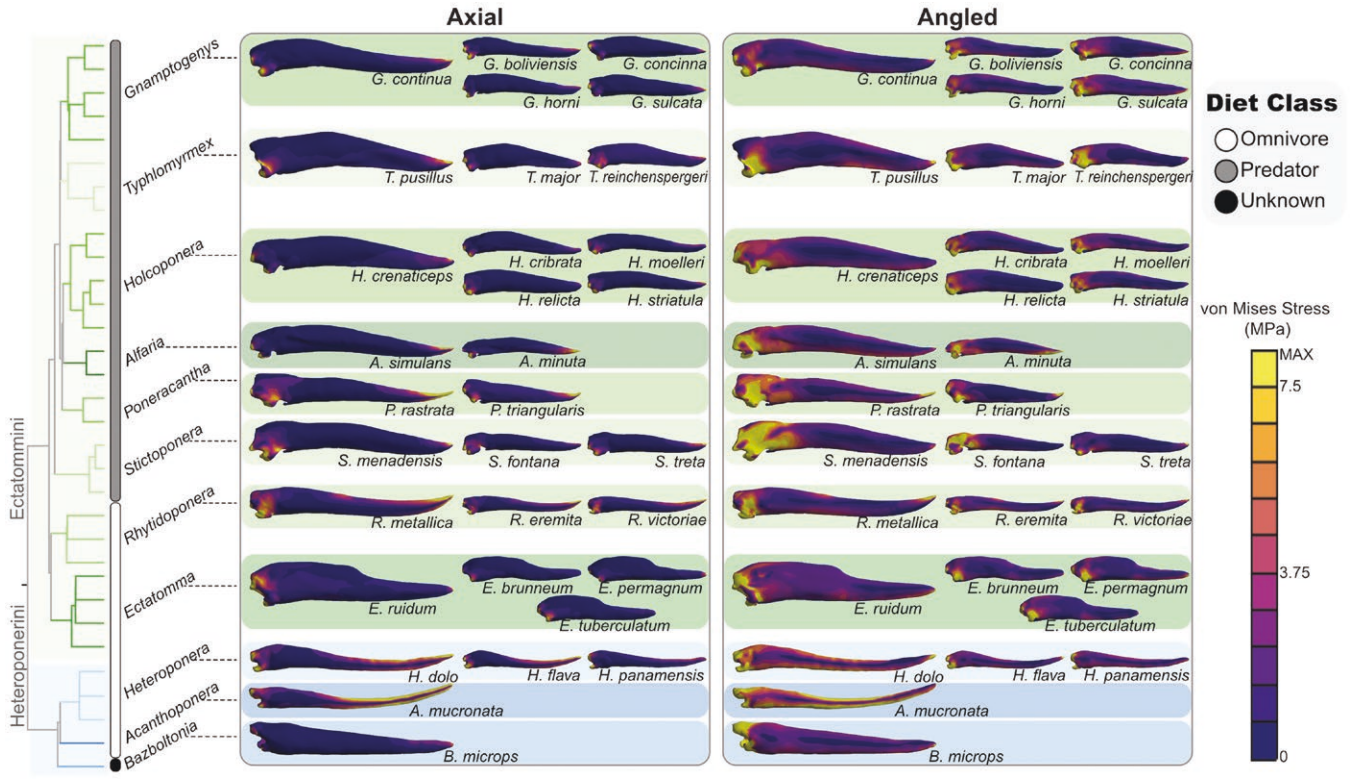

Figure 4. Von Mises stress distribution on the stinger of Ectatomminae represented in a modified phylogeny from Camacho et al. (2022). The scale was manually adjusted so that the brightest areas represent von Mises stress values > 7.5 MPa in each puncture loading condition (axial and angled). The stinger tip and base showed the highest stresses; in contrast, the central axis of the stinger showed the lowest values. The stress distribution pattern indicated that short and straighter stingers experience compression, whereas long, slender, and dorsally curved stingers experience bending. Vertical bars indicate different diet classes (omnivore [white], predator [gray], and unknown [black]).

and performance metrics. Ancestral state reconstructions of diet class (omnivore, predator, and unknown) were estimated based on maximum likelihood (Pagel, 1994) using the R package APE v. 5.8 (Paradis et al., 2004) with an equal-rate (ER), all-rates-different (ARD), and symmetrical (SYM) model for the transition rate among character states, and the best fitting model was identified using Akaike Information Criterion corrected for small sample sizes (AICc).

Combined performance surfaces

Performance surfaces were mapped over a bivariate phylomorphospace (limited to PC1 and PC2) of stinger shape to understand the relationship between morphological and functional variations. We standardized the MWAM and critical buckling load (i.e., in the following equation representing *performance*) each by scaling the variance between 0 and 1, where 0 indicates the lowest performance, and 1 represents the highest performance (*Rescaled performance* = 1 – [*Raw performance – Minimum observed raw performance*]/[*Maximum observed raw performance – Minimum observed raw performance*]) (Polly et al., 2016; Stayton, 2019). Combined performance surface analyses were conducted using the Morphoscape v. 1.0.1 package (Dickson et al., 2021). Performance variables, including puncture loading conditions and critical buckling load, were transformed into performance surfaces using the "krige_surf" function. Combined performance surfaces were calculated by merging the individual performance surfaces across all possible permutations of weights, ranging from 0 to 1 in increments of 0.005, resulting in 1,373,701 landscapes through the "calc_all_lscps" function. The "calcGrpWprime" function was then used to identify the top 5% of weight combinations that yielded the highest overall fitness value (*Z*) across all surfaces, generating an optimally weighted combined performance surface.

Results

Variation in stinger shape

Principal component analysis revealed that the occupation of the phylomorphospace was primarily driven by a divergence in the first principal component (PC1) scores between the two major Ectatomminae lineages (Heteroponerini [which encompass *Acanthoponera*, *Bazboltonia*, and *Heteroponera*] and Ectatommini [which includes all the remaining lineages]), with a single convergence (i.e., *Rhytidoponera* with Heteroponerini) (Figure 3). Some ectatommine lineages were constrained to small regions of the phylomorphospace, whereas *Gnamptogenys*, *Holcoponera*, *Stictoponera*, and *Typhlomyrmex* occupied both low and high scores in the second principal component axis (PC2) (Figure 3).

PC1 accounted for 61.12% of the total variance in shape (Figure 3) and described the length, slenderness, and curvature of the stylet; the angle and position of the proximodorsal process of the stinger bulb; and the height of the stinger base. *Acanthoponera*, *Heteroponera*, and *Rhytidoponera* scored high on PC1 (Figure 3), representing at least two independent origins of the long, slender, and dorsal curved stingers in

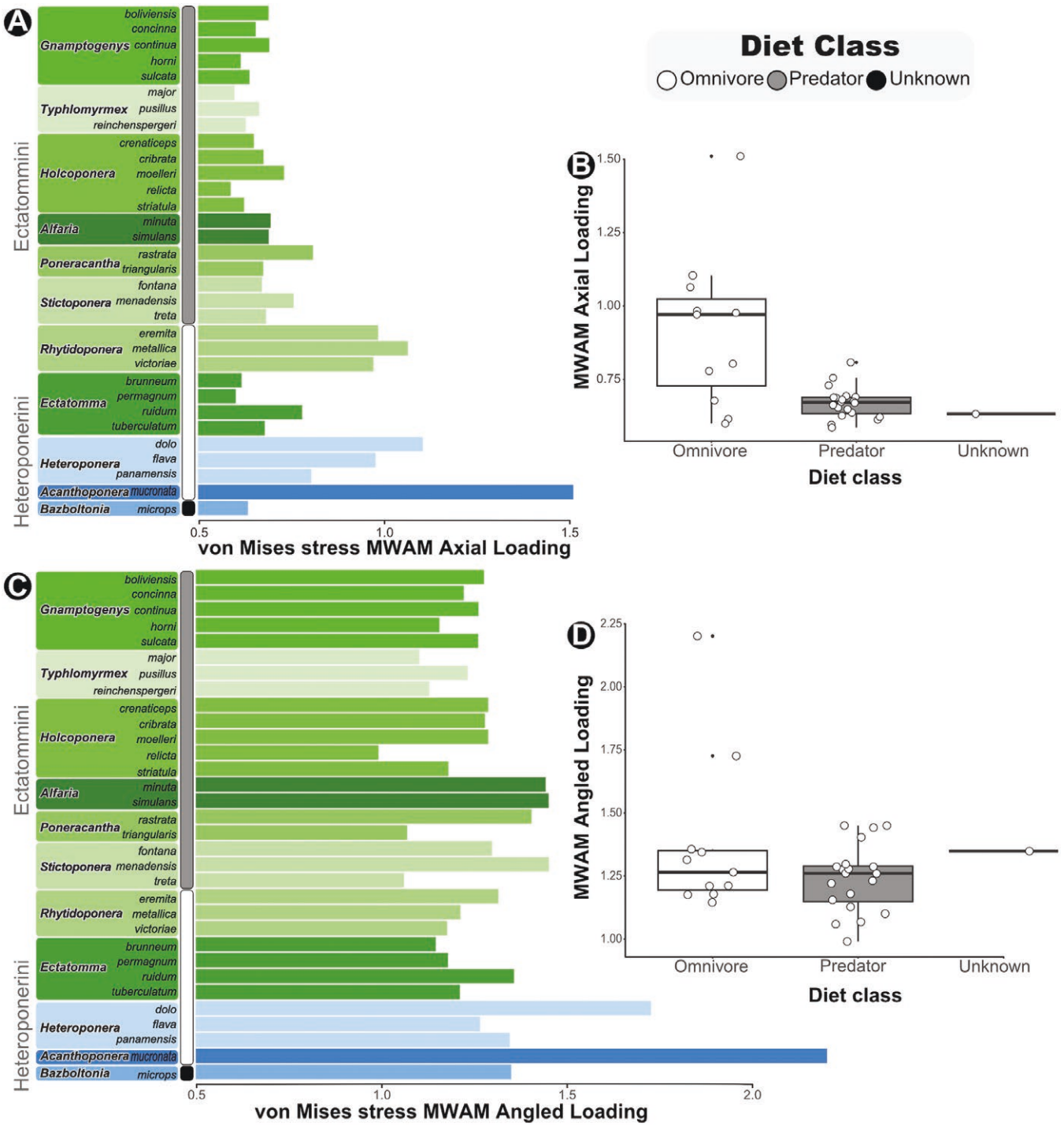

Figure 5. The mesh-weighted arithmetic mean of von Mises stress (MWAM) of the stinger of Ectatomminae of each taxon for (A) axial loading and (C) angled loading conditions. Box plots show the median and range of MWAM across diet classes (omnivores, predators, and unknown) under (B) axial loading and (D) angled loading conditions, highlighting lower mechanical resistance and a wider dispersion among omnivores in the case of axial loading, whereas no differences were observed under angled loading conditions. It is important to emphasize that in this plot, the only species for which the diet class is unknown is *B. microps*, whose biology remains a mystery. Vertical bars in (A) and (C) indicate different diet classes (omnivore [white], predator [gray], and unknown [black]).

Ectatomminae. *Bazboltonia* also scored high on PC1 (Figure 3), possibly because of stinger elongation (i.e., protrusion of the proximodorsal process of the stinger bulb). Nevertheless, its stylet was straighter than that of other Heteroponerini phenotypes. In contrast, *Ectatomma*, *Typhlomyrmex*, and some lineages of *Gnamptogenys*, *Holcoponera*, and *Stictoponera* showed low PC1 scores, suggesting at least five independent origins of short, stout, and almost straight stingers (Figure 3). Finally, *Alfaria*, *Poneracantha*, and the remaining lineages of *Gnamptogenys*, *Holcoponera*, and *Stictoponera* exhibited intermediate scores (Figure 3) associated with compact and slightly curved phenotypes.

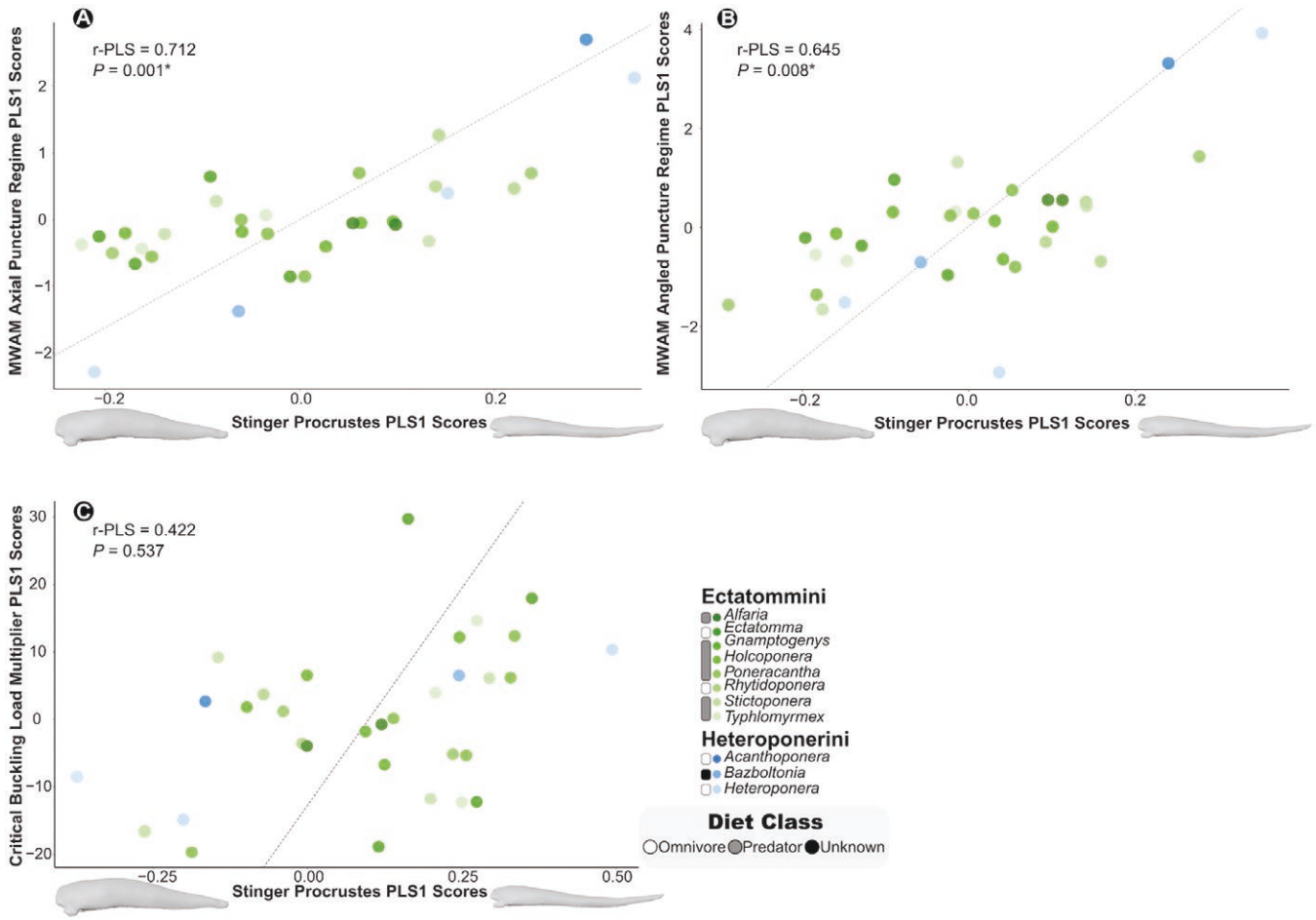

Figure 6. The plot of phylo-PLS showing a positive covariation associated with stinger shape (Procrustes) and mesh-weighted arithmetic mean of von Mises stress (MWAM) resulting from (A) axial, (B) angled puncture loading conditions, and (C) critical buckling load. Stinger models show the warped 3D model associated with minimum (short and robust stingers) and maximum (long and slender stingers) PLS vector scores. Vertical bars indicate different diet classes (omnivore, predator, and unknown).

PC2 accounted for 13.25% of the total variance in shape (Figure 3) and was dominated by the ventral curvature of the stinger and extension of the articular process of the stinger bulb, and along with PC1, the elongation of the stylet. *Alfaria* and most members of *Gnamptogenys*, *Holcoponera*, and *Stictoponera* scored high on PC2 (Figure 3). These lineages had slightly elongated stylets, ventrally curved stingers (in contrast to those of *Acanthoponera* and *Heteroponera* whose stylet was dorsally curved), and a protuberant articular process of the stinger bulb. All other clades showed low scores on PC2, with the articular process of the stinger bulb not protuberant. Regions of both high and low PC2 scores were occupied by phylogenetically distant lineages, indicating multiple independent origins of these phenotypes in Ectatomminae.

The final two principal component axes (PC3, 7.08%; and PC4, 5.75% of the total variance), as indicated by the broken-stick model, described the stinger bulb height and the distance between the proximodorsal process and margin of the stinger bulb (Supplementary Electronic Material, Figure S1).

Biomechanical performance

The distribution of von Mises stress in the finite element models revealed similar patterns under both loading conditions (axial and angled) (Figure 4). The tip of the stinger (i.e., puncture force location) and its base (i.e., boundary location) showed the highest stress, whereas, in all models, the central axis of the stinger showed the lowest stress (Figure 4). Stingers with a deep ventral concavity near the articular process (e.g., *Poneracantha* and *Stictoponera*) showed high stress along the bulb region, which became more obvious under the angled loading condition (Figure 4). Straight and short stylets (e.g., *Bazboltonia* and *Ectatomma*), as well as stingers that were slightly curved ventrally (e.g., *Alfaria*, *Gnamptogenys*, *Holcoponera*, *Stictoponera*, and *Typhlomyrmex*) experienced generally low stress with a pattern consistent with compression (Figure 4). In contrast, slender stingers with dorsally curved stylets, such as those of *Acanthoponera*, *Heteroponera*, and *Rhytidoponera*, experienced higher stress along the dorsal and ventral edges of the stylet, and its center showed lower stress (Figure 4), a configuration similar to the bending of a cantilever beam. Models under the angled loading condition experienced higher stress than those under the axial loading condition (Figure 4).

The MWAM under the axial loading condition was substantially higher in omnivore species than in predators, also showing the largest range of variation (Figure 5A and B). In contrast, under angled loading conditions, MWAM showed no clear differences (Figure 5C and D). Shorter, stouter stingers showed lowest stress values in axial loading (e.g., *Alfaria*, *Ectatomma*, *Gnamptogenys*, *Holcoponera*, *Poneracantha*,

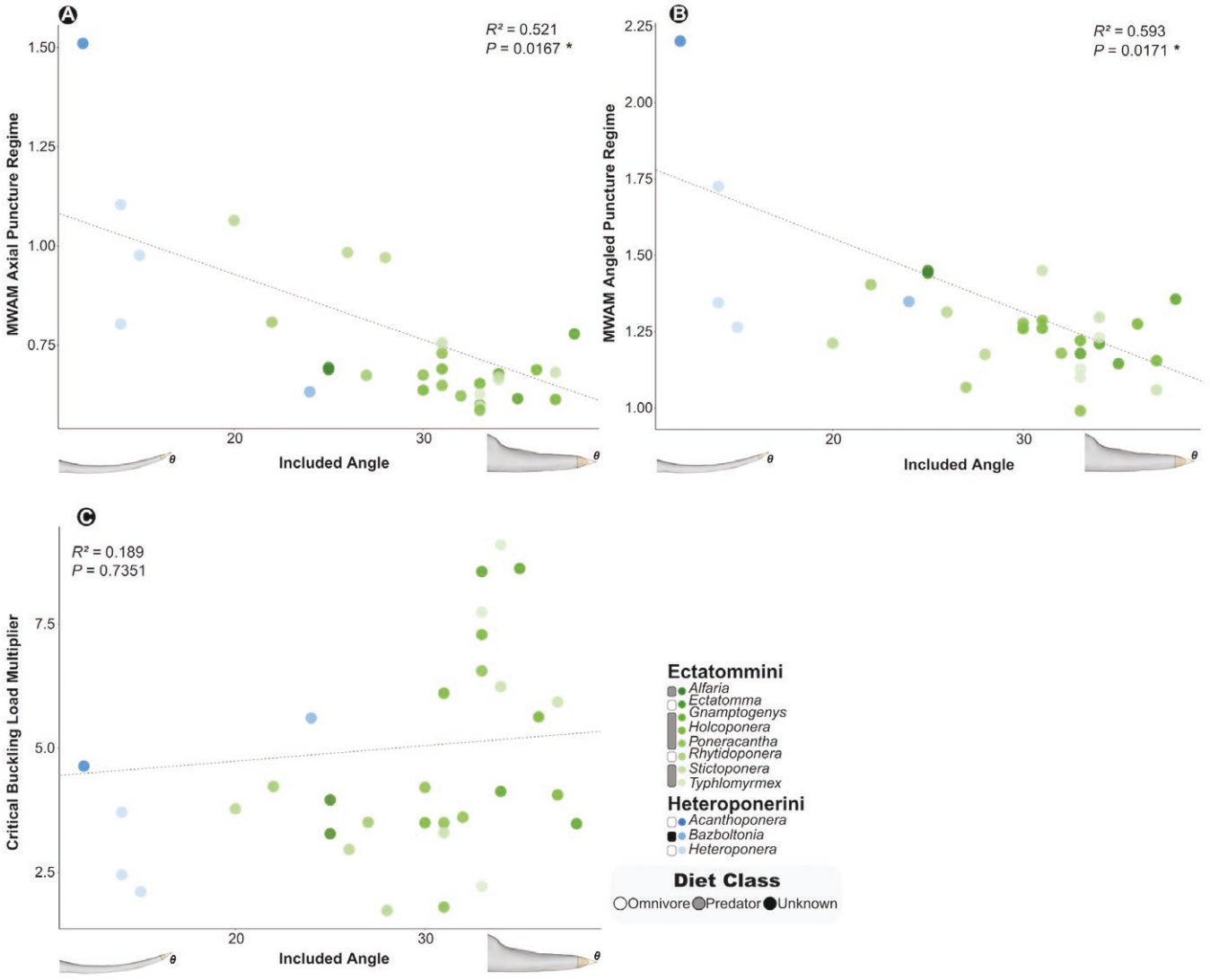

Figure 7. The plot of PGLS showing the relationship between included angle and performance metrics (mesh-weighted arithmetic mean of von Mises stress (MWAM) and critical buckling load). Results are from (A) axial, (B) angled puncture loading conditions, and (C) critical buckling load. Stinger models show generalized stingers with small to large included angles on the X-axis. Vertical bars indicate different diet classes (omnivore, predator, and unknown).

Stictoponera, and *Typhlomyrmex*) (Figure 5A), whereas elongated stingers showed highest values (e.g., *Acanthoponera*, *Heteroponera*, and *Rhytidoponera*) (Figure 5A).

Correlation between phenotype and functional performances

No significant covariation between stinger shape and critical buckling load was found (r-PLS = 0.422, $p = 0.537$; Figure 6C). However, significant and positive covariation was observed for the axial (r-PLS = 0.712, $p = 0.001$; Figure 6A) and angled (r-PLS = 0.645, $p = 0.008$; Figure 6B) puncture loading conditions.

Most of the covariation was driven by stinger elongation and the dorsal curvature of the stylet drive, with the resultant MWAM for axial (Figure 6A) and angled (Figure 6B) punctures. Species in the negative part of the axial loading condition plot (Figure 6A) had short, stout, and straight stingers (low PC1 scores) that performed better under this loading condition (lower MWAM values). Conversely, species in the positive part of the axial loading condition plot (Figure 6A) had long, slender, and dorsal curved stingers (high PC1 scores) that performed poorly under this loading condition (high MWAM values). The angled puncture loading condition plot showed a similar covariation pattern between stinger shape and MWAM values (Figure 6B).

A significant relationship between the traits while accounting for phylogenetic relatedness was found ($F = 6.422$, $R^2 = 0.521$, $p < 0.05$ and $F = 6.368$, $R^2 = 0.593$, $p < 0.05$, respectively) (Figure 7A and B). No significance was observed between the included angle and critical buckling load ($F = 0.117$, $R^2 = 0.189$, $p > 0.05$) (Figure 7C). Significant nonlinear relationships between body size and performance measures were observed (Figure 8). The linear term for log-transformed body size was significant ($F = 6.86$, $p = 0.0139$) in axial puncture, while the quadratic term showed borderline significance ($F = 4.10$, $p = 0.0522$), indicating that species with intermediate body sizes had higher maximum stress in axial compression, while smaller and larger species had lower values (Figure 8A). For angled puncture, the linear term was significant ($F = 8.68$, $p = 0.0063$), but

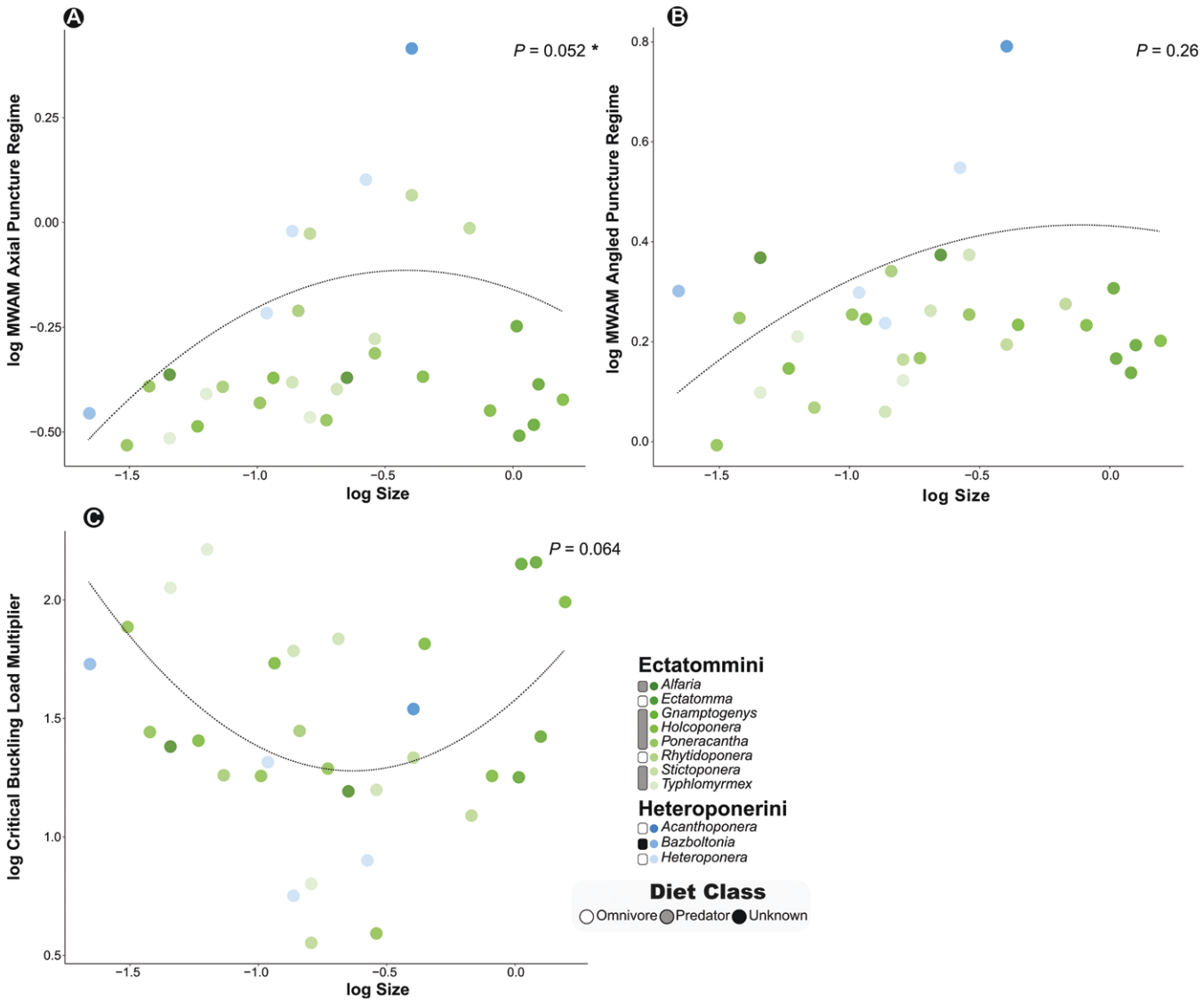

Figure 8. The plot of PGLS results illustrating the relationship between the body size and log of stinger performance metrics: (A) maximum stress in axial compression, (B) angled puncturing regime, and (C) critical buckling load. The X-axis represents the log of body size, measured as the width between the seventh abdominal spiracles. Intermediate-sized species are shown to have weaker mechanical performance in (A) axial compression and (B) angled puncturing. The vertical bars denote different diet classes (omnivore, predator, and unknown).

no significance was found for the quadratic term ($F = 1.32$, $p = 0.2593$), suggesting a weaker direct effect of body size on the angled puncturing regime (Figure 8B). Finally, the quadratic term approached significance ($F = 3.70$, $p = 0.0644$) for critical buckling, indicating a potential nonlinear relationship with body size (Figure 8C).

Shifts in phenotype and functional trait regimes

For phenotype, two locations on the phylogeny had regime shifts occurred toward longer and slender stingers (*Rhytidoponera* and Heteroponerini), and two shifts occurred toward short and stout stingers (*Ectatomma* and *Typhlomyrmex*) with a posterior probability of > 0.4 (Figure 9A and B). Moreover, the two regime shifts were located toward lineages with small included angles (*Rhytidoponera* and Heteroponerini; *pp* > 0.4, Figure 9C and D). Remarkably, the regime shifts in phenotype were predominantly associated with omnivore lineages (Heteroponerini, *Ectatomma*, and *Rhytidoponera*) (Figure 9A and C), except for one PC1 shift associated with the predatory lineage *Typhlomyrmex* (Figure 9A). Based on our maximum likelihood estimation of the ancestral discrete character using ER (AICc: ER = 21.61; ARD = 26.89; SYM = 23.84), it is possible that Ectatomminae had omnivore ancestors (omnivore = 0.923; predator = 0.062; unknown = 0.015) (Figure 9A and B).

For performance traits, five regime shifts related to the axial loading condition (*Rhytidoponera*, *Poneracantha*, *Acanthoponera*, and two in *Heteroponera*; *pp* > 0.4, Figure 9E and F) and three shifts for the angled loading condition (*Alfaria*, *Acanthoponera*, and *Heteroponera*; *pp* > 0.4, Figure 9G and H) were identified, all toward high MWAM values. Conversely, five regime shifts were revealed toward lineages with high critical buckling loading (*Ectatomma*, *Gnamptogenys*, *Typhlomyrmex*, *Holcoponera*, and *Stictoponera*; *pp* > 0.4, Figure 9I and J). Remarkably, the regime shifts in axial and angled loading conditions exhibited a consistent pattern as those found for phenotype, with most shifts occurring toward omnivore lineages (e.g., *Acanthoponera*, *Heteroponera*, and

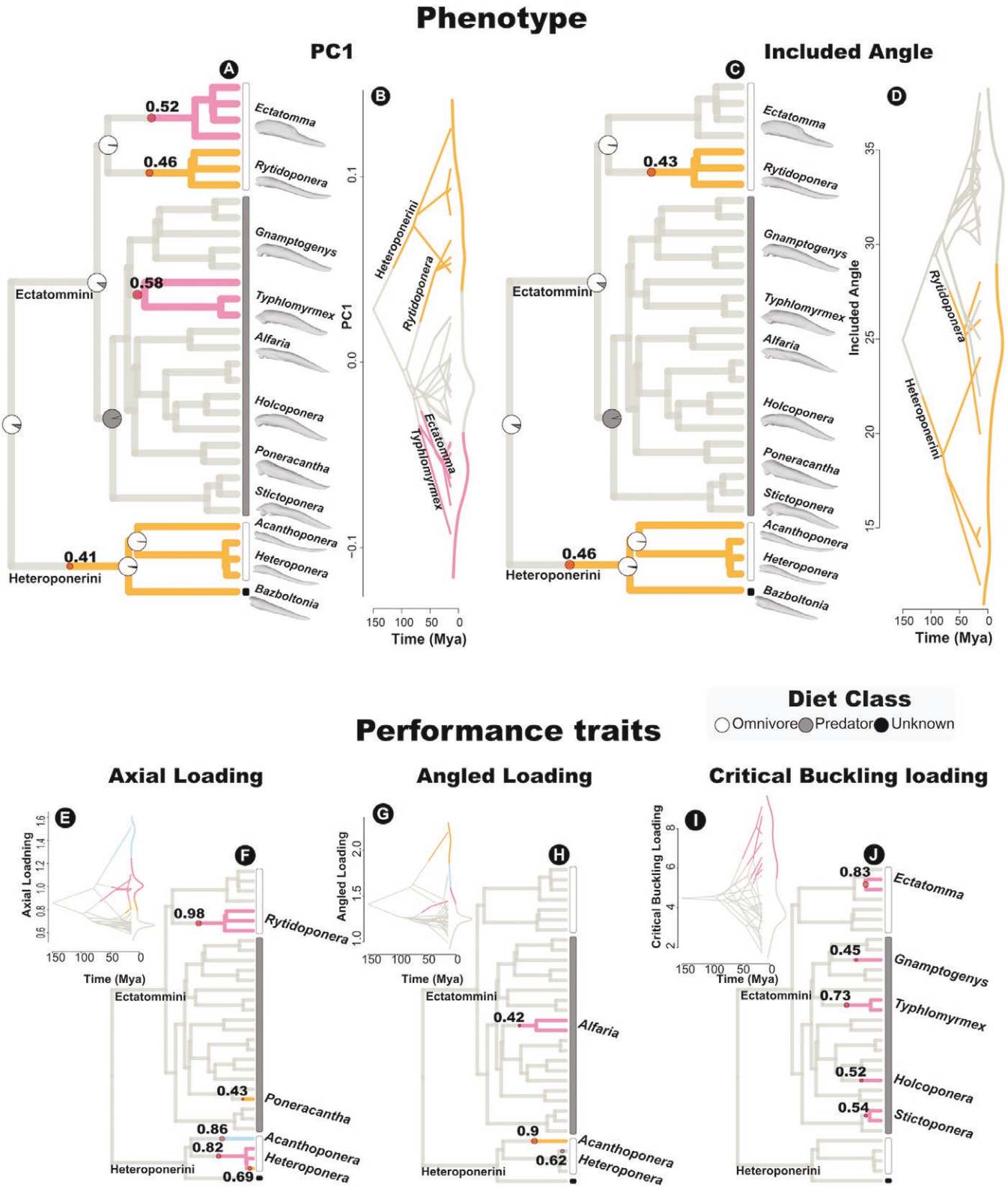

Figure 9. Ectatomminae phylogeny showing trait regimes of a BAYOU rjMCMC analysis. Branches with similar colors represent branches with convergent regimes for phenotype, as illustrated by (A) PC1 and (C) included angle and performance traits, characterized by (F) axial, (H) angled, and (J) critical buckling loading. Different-sized circles show the location and posterior probability of a regime shift. Phenograms (B, D, E, G, and I) illustrate density and estimated evolutionary history based on lineage-specific rates of evolution. Vertical bars indicate different diet classes (omnivore, predator, and unknown). Pier charts at the nodes of the phylogeny in (A) and (B) indicate the maximum likelihood of ancestral character reconstruction of diet class (discrete trait) in Ectatomminae using the ER (best-fitted model AICc = 21.61) model of evolution.

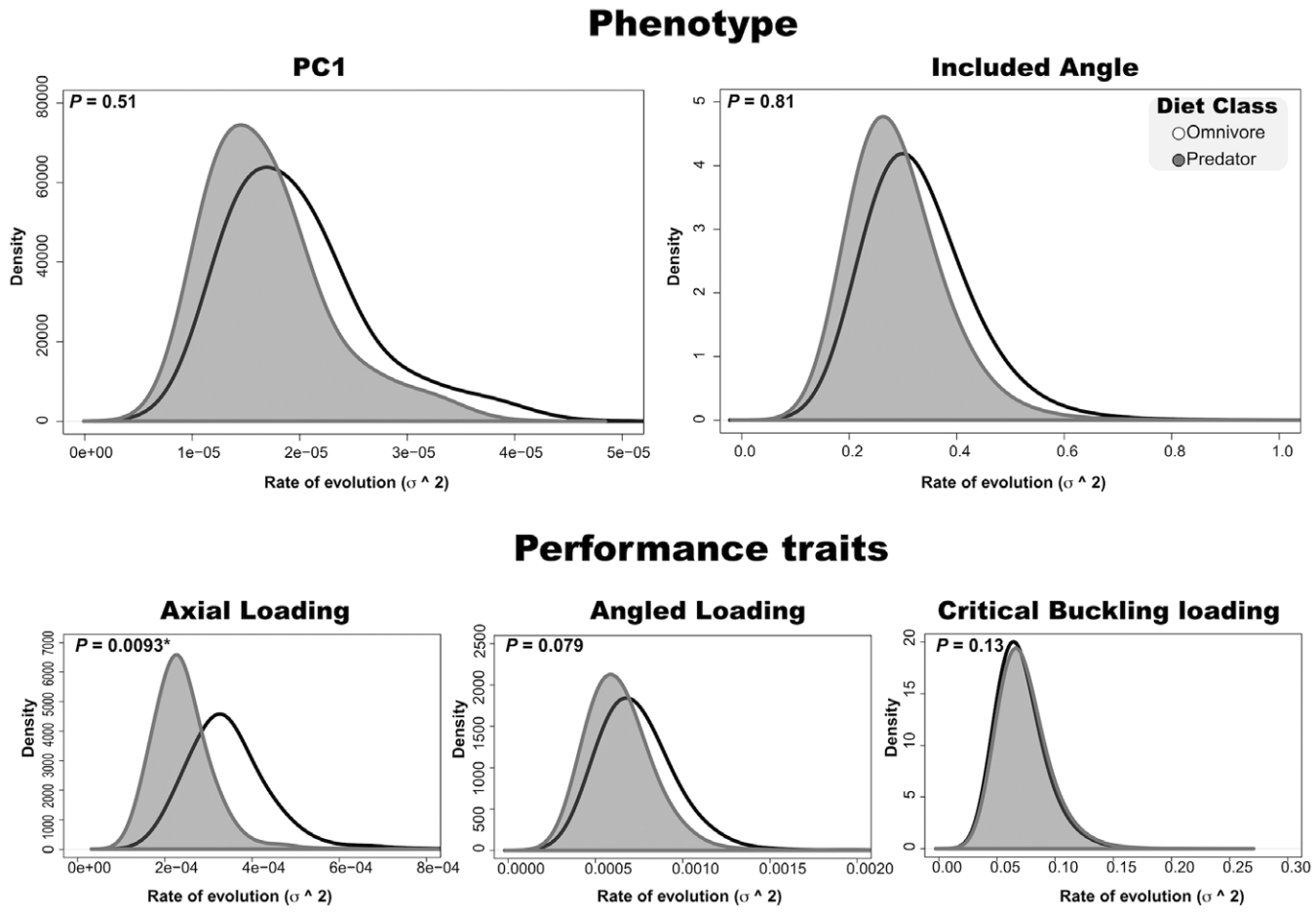

Figure 10. Rate of evolution ($\sigma 2$) of phenotype (PC1 and included angle) and performance traits (axial, angled, and critical buckling loading) for different diet classes (omnivore and predator) as estimated by a standard Brownian motion model.

Rhytidoponera for axial loading and *Acanthoponera* and *Heteroponera* for angled loading). In contrast, regime shifts for critical buckling loading were primarily observed in predatory lineages (*Gnamptogenys*, *Holcoponera*, *Stictoponera*, and *Typhlomyrmex*), with only a single shift occurring toward an omnivore lineage (*Ectatomma*).

The difference in the rate of evolution between omnivore and predatory lineages was significant for the axial loading condition ($p = 0.0093$) at a ratio of 6.86 (omnivore $\sigma^2 = 0.00115$, predatory $\sigma^2 = 0.00017$) (Figure 10). There were no differences in the rate of evolution for morphology (PC1 $p = 0.51$, included angle $p = 0.81$) and the remaining performance traits (angled loading condition $p = 0.079$ and critical buckling loading $p = 0.13$) (Figure 10).

Phylomorphofunctional landscape

The range of simulated axial and angled puncture loading conditions mapped to similar performance surfaces within the phylomorphospace (Figure 11A), in contrast to critical buckling load, which mapped performance surfaces represented by smaller islands of higher performance. A combined performance surface resulted in a mapping with the same pattern as that under axial and angled puncture loading conditions (Figure 11B) (estimate contribution weights: axial = 0.70,269; angled = 0.25,765), most probably due to the higher contribution of axial loading conditions than that by critical buckling load (contribution weight: critical buckling = 0.03966). Ectatommini dominated higher performance areas, whereas Heteroponerini occupied underperforming regions of the combined performance landscape (Figure 11B). Nevertheless, the predominance of Ectatommini in higher-performance regions was not a consistent trend, with *Rhytidoponera* sharing a low-performance boundary with *B. microps* (Heteroponerini). Considering the combined performance landscape, performance increased with short and robust stingers (low PC1 scores), whereas curved, long, and slender stingers (high PC1 scores) performed poorly (Figure 11B). Variations associated with the ventral curvature of the stinger and modifications of the articular process of the stinger bulb (PC2) exerted no influence on the stinger-rescaled performance of the combined performance landscape (Figure 11B).

Discussion

Our results shed light on the functional morphology and evolution of the Hymenoptera stinger and, more generally, on the phenotypic diversification in relation to task specialization. Using a comparative approach within a phylogenomic framework, we investigated for the first time the mechanical responses related to stinger shape variation using a clade of ants (Ectatomminae) as a model system. Although Ectatomminae do not have all the functional and shape variations found across ants, or Hymenoptera, they do differ along

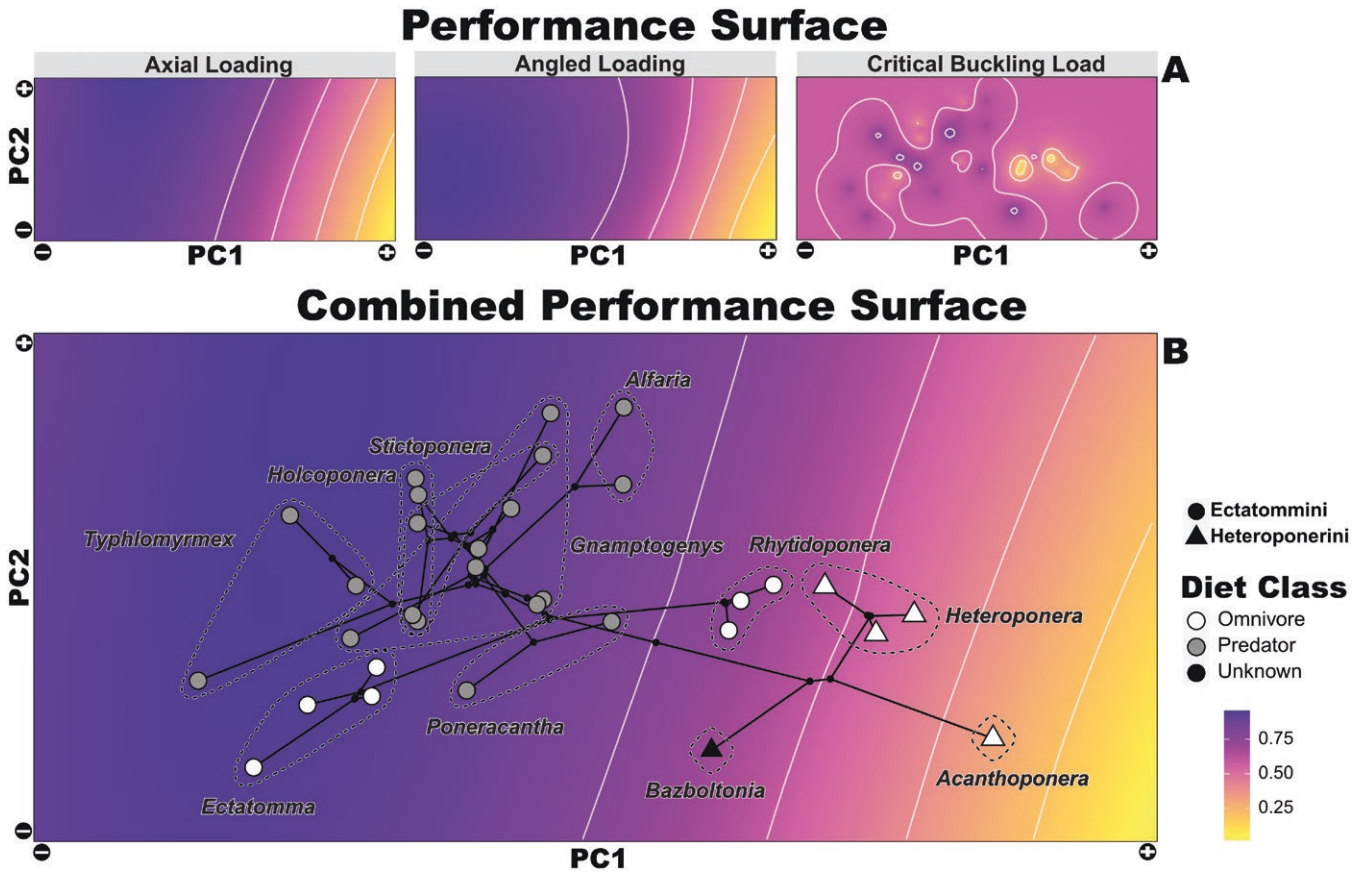

Figure 11. Functional performance surfaces and adaptive landscape. (A) Performance surfaces recovered for the two loading conditions (axial and angled) and critical buckling load measured on the phylomorphospace and (B) adaptive landscape resulted from the combined performance surfaces showing Ectatommini dominating higher performance areas compared with Heteroponerini. A value of 1.0 (dark shades) indicates high performance and a value of 0 (light shades) indicates poor performance.

common axes of variation (elongation and curvature) that are found across the order.

Within Ectatomminae, the divergence between Ectatommini and Heteroponerini is responsible for most of the disparity in stinger shape, with elongation explaining much of the shape variance, followed by the curvature in its distal portion (i.e., the stylet) (Figure 3). Furthermore, both tribes show high shape diversity within their genera, with a higher variation in Ectatommini than in Heteroponerini (Figure 3). We demonstrated that this divergence also reflects the occupancy of the combined performance landscape, with the highly diverse Ectatommini dominating a large region with improved mechanical performance and Heteroponerini clustering in lower performance areas (i.e., areas susceptible to structural mechanical limitations) (Figure 11). A significant nonlinear relationship was found between body size and stinger performance, particularly for axial compression stress (Figure 8). Intermediate-sized species exhibit overall mechanically weaker stinger compared to smaller and larger species. Contrary to what would be expected, increased size does not directly compensate for a structurally weaker stinger. These findings suggest that intermediate-sized species may encounter functional constraints leading to suboptimal stinger strength, while smaller and larger species exhibit more mechanically efficient stingers. Our results also suggested that omnivore species have relatively weaker stingers under axial loading conditions than species that are primarily predators (Figure 5). Nevertheless, omnivore lineages concentrated most regime shifts in phenotype and performance (except for critical buckling loading). No clear tradeoff was observed between ants having short and robust stingers and ants having long and slender stingers. Moreover, no apparent advantages were associated with long and slender stingers, leaving this aspect as an intriguing, unmodeled function that merits further investigation.

Shape diversity of the sting apparatus

Hymenoptera stingers are often considered as one of the targets of natural selection as their functionality is crucial for hunting and defense, individual and/or colonial, in social aculeates. The support for the stinger as a key innovation for the diversification of Hymenoptera is equivocal, as the increased diversification rates in other nonaculeate clades might dilute the signal of a state-dependent diversification associated with the origin of the stinger (Blaimer et al., 2023). Nonetheless, the innovative functions of the stinger may have exerted an impact on accelerating diversification (Blaimer et al., 2023), and shape diversity still needs to be addressed for the Hymenoptera stinger, which is frequently assumed to have a generalized needle-like form (e.g., Bar-On, 2019). In contrast to vertebrate teeth, plant thorns, and cone snail harpoons, which have their internal structure filled with relatively rigid tissue (e.g., dentin for teeth and various plant tissues for thorns), fangs and stingers require an internal

channel through which the venom can flow. Such hollowness allows these morphologies to present relatively high resistance against compression while simultaneously allowing a certain flexibility when loaded angularly (Milwich et al., 2006; Pohl et al., 2020; Zhao et al., 2010). Nevertheless, unlike other venom injection systems, the Hymenoptera stinger presents a complex internal geometry, primarily due to the presence of a stinger bulb apophysis and an inner dorsal wall of the stylet that produces two lateral channels, which converge at the stylet proximal extremity, ultimately merging to form an enclosed central channel (Figure 1E).

Slender and elongated venom injection tools are often associated with specialized and optimized properties for puncturing soft tissues, requiring lower forces for penetration (Ballell et al., 2022; Evans & Sanson, 2003, 2006) but being more susceptible to high average values of von Mises stress and more likely to exceed yield failure criteria. According to their higher stress magnitudes and distribution patterns (Figures 4 and 5), Heteroponerini and *Rhytidoponera* possess the mechanically weakest stingers under simple compression. The reduced mechanical resistance of their stinger to puncture-related loads compared with that of Ectatommini (excluding *Rhytidoponera*) (Figures 5 and 6) is probably due to the different material characteristics of their stinging target. This mechanical pattern suggests that these lineages occasionally prey on soft-bodied invertebrates (e.g., termites) and immature arthropods (e.g., eggs and larvae) (see Vincent & Wegst, 2004 for differences in the material properties of insect cuticles; Vicent, 2002 for general arthropod cuticle) or rarely use their stinger by supplementing their diet with plant derivatives and dead organisms (i.e., detritivores). In addition, we propose that the high likelihood of higher average von Mises stress values can be mitigated through venom with faster and more deleterious activity, aiming to subdue the prey without the need for multiple stings. To the best of our knowledge, only a few studies have described the stinging behavior in Ectatomminae, and the chemical composition of the venom has been described only in *Rhytidoponera metallica* (Smith) and *Ectatomma tuberculatum* (Olivier) (Brophy et al., 1981; Brown et al., 2011; Robinson et al., 2023).

Short, blunt-shaped piercing systems may show low average von Mises stress values when attempting to break through tougher surfaces, similar to that observed with the fangs of crab-feeders Homalopsidae (Cleuren et al., 2021), teeth of omnivorous Sauropodomorphs (Ballell et al., 2022), occlusal variation in durophagous tooth morphologies (Crofts, 2015), and tooth adaptation for shell crushing (Crofts & Summers, 2014). Ectatommini, besides *Rhytidoponera*, exhibited a broad range of robust stinger diversity that can vary from nearly straight (*Ectatomma* and *Poneracantha*) to slightly convex ventrally (*Alfaria*, *Gnamptogenys*, *Holcoponera*, *Stictoponera*, and *Typhlomyrmex*) (Figures 3 and 4). Although several Ectatommini species exhibit submissive and timid behavior (Cupul-Magaña, 2009; Gobin et al., 1998), some groups can be particularly aggressive (Melati & Leal, 2018). Therefore, the short and robust stinger of Ectatommini, mechanically adapted to overcome high loads (Figures 4 and 5), combined with its highly toxic venom (Bernardi et al., 2017; Pluzhinikov et al., 1994; Silva et al., 2018; Touchard et al., 2015), might represent a case of morphological adaptation that enables subduing hostile prey with stiffer teguments and succeeding in agonistic interactions. *Gnamptogenys* is an excellent example of how short and blunt stingers might withstand significant mechanical demand. For instance, the thick and stiff cuticles of fungus-growing ants (Li et al., 2020) with few exposed intersegmental sections represent a challenge for their specialist predator *G. hartmani* to sting.

Our findings demonstrate that the stinger of Hymenoptera exhibits substantial morphological diversity (Figure 3), which causes significant functional variability (Figures 4 and 7). Robust stingers are better at sustaining equivalent stress, increasing their useful life when high-magnitude loads are applied. Remarkably, several lineages occupied suboptimal regions of the morphofunctional space (Figure 11), suggesting that prey selectivity, hostility, stinging behavior, and venom toxicity are crucial mechanisms for mitigating the associated functional demands with a piercing stinger. Our data are consistent with the hypothesis that selective forces related to active hunting, puncturing defense, and prey specialization can result in unique shape variations and improved mechanical functionality.

Effect of dietary preferences on stinger diversification

Our results revealed that the large-scale shifts in phenotypes typically occurred early in the evolutionary history of omnivore lineages, with minor and gradual changes in performance for both omnivores and predators occurring toward the tips of the phylogenetic tree. These data illustrate a strong correlation between shifts in stinger phenotype, performance traits, and trophic evolution. Remarkably, the omnivorous Ectatomminae, which feed on diets rich in plant-based materials such as seed arils and honeydew, showed a higher frequency of regime shifts (Figure 9) than other lineages. These shifts were accompanied by accelerated rates of morphological evolution in performance metrics, particularly in MWAM values for axial and angled loadings (Figure 10). In adaptive radiation scenarios, a tendency toward niche specialization is anticipated when ecological opportunities result in the occupation of new adaptive zones and subsequent niche differentiation as lineages diversify (Simpson, 1953; Stroud & Losos, 2016). Nevertheless, we observed an overall trend toward omnivory (Figures 9 and 10) rather than specialization. Hence, morphological evolutionary patterns are related to the diversification of diets among most Ectatomminae. These results contradict our initial hypothesis of a general trend toward specialization; nonetheless, previous research has demonstrated that trophic specialization toward herbivory correlates with increased speciation rates (Burin et al., 2016; Price et al., 2012; Wiens et al., 2015).

Our results suggest that omnivorous lineages that primarily consume plants are favored over predatory lineages, possibly because a varied diet can help them better adapt to seasonal and spatial resource variations. The evolution of Ectatomminae indicates a transition toward a more limited diet in predatory lineages from an ancestral omnivorous state (Figure 9A and B). As omnivore populations begin specializing in predatory behaviors, they face intense competition from specialist populations, and on a larger scale, niche-filling may limit the exploration of new adaptive zones (McPeek, 2008; Schluter, 2000). The morphological variability in predatory lineages might be insufficient to adapt to new selective pressures (Day et al., 2016), as evidenced by the fewer regime shifts observed in most predatory Ectatomminae (Figure 9). Importantly, although predatory lineages have a more restricted diet (i.e., primarily focused on soft-bodied

invertebrates), their habits are not necessarily specialized. Several species exhibit a broad diet in terms of the prey they can use as food sources, which, in turn, might not lead to morphological specialization.

The dispersion of higher stress values due to feeding-related forces of omnivore species than those of predators (Figure 5), for instance, is probably related to stinger release as the primary tool used for food acquisition. Releasing the stinger as a primary tool for hunting would result in the emergence of forms that are either not adapted to pierce through target tegument or highly adapted to other functions (e.g., trail marking) and/or piercing specific organisms (e.g., soft body invertebrates). Furthermore, besides a few lineages, such as *Rhytidoponera metallica*, that are more aggressive toward other ants and bigger threats (e.g., vertebrates), most omnivore species tend to be shy and rarely sting. We propose that omnivorous species depend on other structures, such as their mandibles, to subdue their prey. Recent studies on the mechanics of ant mandibles have demonstrated that species commonly associated with omnivorous habits have mandibles adapted for abrasive processes (Klunk et al., 2021, 2023), which are not limited to plant consumption. For instance, major workers of the ant genus *Pheidole*, whose stinger is nonfunctional (Kugler, 1979), have highly adapted mandibles for processing hard items, such as breaking seeds and tearing apart invertebrate cuticles. These mandibles are primarily associated with their specialization as food processors but are often used for capturing, restraining, subduing, and dismembering the prey (Dejean et al., 2007; Fowler, 1987; Gomes et al., 2019, 2021) without the need for a functional stinger.

Conclusions

Our results highlight the tradeoffs shaping the evolution of stingers and puncture tools in Hymenoptera and other animals. These structures serve as intriguing models for evolutionary biomechanics, considering the biophysical challenges of puncture and venom delivery, as well as their integration with the behavioral ecology of organisms. Although our study advances the basic understanding of stinger biomechanics, further studies are required to fully understand these complex structures from physical, fluidic, and anatomical perspectives. Furthermore, our results emphasize intriguing associations between diet specialization and functional diversification. Continued research, using diverse analytical approaches and a broader phylogenetic scale, is essential to gain a complete understanding of the diversification of these remarkable structures and their implications for our comprehension of evolutionary processes.

Supplementary material

Supplementary material is available online at *Evolution*.

Data availability

Supporting figures are available as Supplementary Material. All 3D models (.stl) and trimmed phylogeny (.tre) are deposited in the Dryad Digital Repository (https://doi.org/10.5061/dryad.15dv41p5w). The 16 Ectatomminae specimens scanned in the KIT are part of the "Antscan" project and will be made publicly available at https://www.antscan.info.

Author contributions

A.C.F. and E.P.E. conceived the study. A.C.F. prepared the X-ray µCT at OIST, processed the scan data, landmarked models, created the finite element models, analyzed the results, and drafted the first manuscript version. G.P.C., J.E.L., and R.M.F. prepared specimens for scanning and produced the phylogeny. K.T. prepared the X-ray µCT at KIT. G.P.C., K.T., J.E.L., R.M.F., and E.P.E. contributed to the writing of the final manuscript and gave final approval before submission.

Funding

Okinawa Institute of Science and Technology Graduate University, A.C.F. was funded by Japan Society for the Promotion of Science (JPSP)—Grants-in-Aid for Early-Career Scientists KAKENHI (grant 24K18174), and R.M.F. was funded by the Brazilian Council of Research and Scientific Development—CNPq (grant 301495/2019-0).

Conflict of interest: The authors declare no conflict of interest.

Acknowledgements

We thank Alexander Blanke, David Labonte, Jamie Kass, Jeroen Smaers, Jordi Marcé-Nogué, Philip Anderson, Rolf Beutel, and Sanjay Sane for their invaluable analytical suggestions. We thank Miriam Zelditch, Tristan Stayton, and four anonymous reviewers for crucial comments on this manuscript. We thank Charles Kugler for encouraging the execution of this project and Julian Katzke, Adrian Richter, Christine Sosiak, and Shubham Gautam for their insightful discussions throughout the development of this article. We thank Jack Longino for sending specimens from Mesoamerica and Alan Andersen, Juanita Rodriguez, Francisco Hita-Garcia, and Olivia Evangelista for sending specimens from Australia. We thank the Okinawa Institute of Science and Technology Graduate University (OIST) Imaging Section for providing access to the Zeiss Xradia micro-CT scanner and Shinya Komoto for general support. We acknowledge the KIT Light Source for the provision of instruments at their beamlines and we would like to thank the Institute for Beam Physics and Technology (IBPT) for the operation of the storage ring, the Karlsruhe Research Accelerator (KARA).

References

Adams, D. C. (2014). Quantifying and comparing phylogenetic evolutionary rates for shape and other high-dimensional phenotypic data. *Systematic Biology*, *63*(2), 166–177. https://doi.org/10.1093/sysbio/syt105

Adams, D. C., & Collyer, M. L. (2016). On the comparison of the strength of morphological integration across morphometric datasets. *Evolution*, *70*(11), 2623–2631. https://doi.org/10.1111/evo.13045

Adams, D. C., & Collyer, M. L. (2018). Multivariate phylogenetic comparative methods: Evaluations, comparisons, and recommendations. *Systematic Biology*, *67*(1), 14–31. https://doi.org/10.1093/sysbio/syx055

Adams, D. C., & Collyer, M. L. (2019). Phylogenetic comparative methods and the evolution of multivariate phenotypes. *Annual Review of Ecology, Evolution, and Systematics*, *50*(1), 405–425. https://doi.org/10.1146/annurev-ecolsys-110218-024555

Adams, D. C., & Felice, R. N. (2014). Assessing trait covariation and morphological integration on phylogenies using evolutionary covariance matrices. *PLoS One*, *9*(4), e94335. https://doi.org/10.1371/journal.pone.0094335

Anderson, P. S. (2018). Making a point: Shared mechanics underlying the diversity of biological puncture. *Journal of Experimental Biology*, *221*(22), jeb187294. https://doi.org/10.1242/jeb.187294

Arnold, S. J. (1992). Constraints on phenotypic evolution. *The American Naturalist*, *140*(Suppl 1), S85–S107. https://doi.org/10.1086/285398

Baken, E. K., Collyer, M. L., Kaliontzopoulou, A., & Adams, D. C. (2021). Geomorph v4. 0 and gmShiny: Enhanced analytics and a new graphical interface for a comprehensive morphometric experience. *Methods in Ecology and Evolution*, *12*(12), 2355–2363. https://doi.org/10.1111/2041-210x.13723

Ballell, A., Benton, M. J., & Rayfield, E. J. (2022). Dental form and function in the early feeding diversification of dinosaurs. *Science Advances*, *8*(50), eabq5201. https://doi.org/10.1126/sciadv.abq5201

Bar-On, B. (2019). On the form and bio-mechanics of venom-injection elements. *Acta Biomaterialia*, *85*, 263–271. https://doi.org/10.1016/j.actbio.2018.12.030

Bernardi, R. C., Firmino, E. L. B., Mendonça, A., Sguarizi-Antonio, D., Pereira, M. C., da Cunha Andrade, L. H., Antonialli-Junior, W. F., & Lima, S. M. (2017). Intraspecific variation and influence of diet on the venom chemical profile of the *Ectatomma brunneum* Smith (Formicidae) ant evaluated by photoacoustic spectroscopy. *Journal of Photochemistry and Photobiology B: Biology*, *175*, 200–206. https://doi.org/10.1016/j.jphotobiol.2017.09.004

Bertram, J. E., & Biewener, A. A. (1988). Bone curvature: Sacrificing strength for load predictability? *Journal of Theoretical Biology*, *131*(1), 75–92. https://doi.org/10.1016/s0022-5193(88)80122-x

Bhushan, B. (2018). Insects locomotion, piercing, sucking and stinging mechanisms. In *Biomimetics* (pp. 819–860). Springer.

Blaimer, B. B., Santos, B. F., Cruaud, A., Gates, M. W., Kula, R. R., Mikó, I., Rasplus, J. Y., Smith, D. R., Talamas, E. J., Brady, S. G., & Buffington, M. L. (2023). Key innovations and the diversification of Hymenoptera. *Nature Communications*, *14*(12121), 18. https://doi.org/10.1038/s41467-023-36868-4

Bolton, B. (2024). An online catalog of the ants of the world. https://antcat.org. Date accessed January 10th, 2023.

Botton-Divet, L., Cornette, R., Fabre, A. C., Herrel, A., & Houssaye, A. (2016). Morphological analysis of long bones in semi-aquatic mustelids and their terrestrial relatives. *Integrative and Comparative Biology*, *56*(6), 1298–1309. https://doi.org/10.1093/icb/icw124

Brophy, J. J., Cavill, G. W. K., & Plant, W. D. (1981). Volatile constituents of an Australian ponerine ant *Rhytidoponera metallica*. *Insect Biochemistry*, *11*(3), 307–310. https://doi.org/10.1016/0020-1790(81)90008-1

Brown, S. G., Van Eeden, P., Wiese, M. D., Mullins, R. J., Solley, G. O., Puy, R., Taylor, R. W., & Heddle, R. J. (2011). Causes of ant sting anaphylaxis in Australia: The Australian ant venom allergy study. *The Medical Journal of Australia*, *195*(2), 69–73. https://doi.org/10.5694/j.1326-5377.2011.tb03209.x

Burin, G., Kissling, W. D., Guimaraes P. R. Jr, Şekercioğlu, C. H., & Quental, T. B. (2016). Omnivory in birds is a macroevolutionary sink. *Nature Communications*, *7*(11250), 1–10. https://doi.org/10.1038/ncomms11250

Camacho, G. P., Franco, W., Branstetter, M. G., Pie, M. R., Longino, J. T., Schultz, T. R., & Feitosa, R. M. (2022). UCE phylogenomics resolves major relationships among ectaheteromorph ants (Hymenoptera: Formicidae: Ectatomminae, Heteroponerinae): A new classification for the subfamilies and the description of a new genus. *Insect Systematics and Diversity*, *6*(1), 5. https://doi.org/10.1093/isd/ixab026

Cleuren, S. G., Hocking, D. P., & Evans, A. R. (2021). Fang evolution in venomous snakes: Adaptation of 3D tooth shape to the biomechanical properties of their prey. *Evolution*, *75*(6), 1377–1394. https://doi.org/10.1111/evo.14239

Crofts, S. (2015). Finite element modeling of occlusal variation in durophagous tooth systems. *The Journal of Experimental Biology*, *218*(Pt 17), 2705–2711. https://doi.org/10.1242/jeb.120097

Crofts, S. B., Lai, Y., Hu, Y., & Anderson, P. S. L. (2019). How do morphological sharpness measures relate to puncture performance in viperid snake fangs? *Biology Letters*, *15*(4), 20180905. https://doi.org/10.1098/rsbl.2018.0905

Crofts, S. B., & Summers, A. P. (2014). How to best smash a snail: The effect of tooth shape on crushing load. *Journal of the Royal Society Interface*, *11*(92), 20131053. https://doi.org/10.1098/rsif.2013.1053

Cupul-Magaña, F. G. (2009). First observation of defensive behavior by death feigning in the ant *Ectatomma ruidum* (Roger, 1861) (Formicidae, Ponerinae). *Acta Zoológica Mexicana*, *25*(1), 199–201.

Day, E. H., Hua, X., & Bromham, L. (2016). Is specialization an evolutionary dead end? Testing for differences in speciation, extinction and trait transition rates across diverse phylogenies of specialists and generalists. *Journal of Evolutionary Biology*, *29*(6), 1257–1267. https://doi.org/10.1111/jeb.12867

Dejean, A., Moreau, C. S., Uzac, P., Le Breton, J., & Kenne, M. (2007). The predatory behavior of *Pheidole megacephala*. *Comptes Rendus Biologies*, *330*(9), 701–709. https://doi.org/10.1016/j.crvi.2007.06.005

Denton, J. S., & Adams, D. C. (2015). A new phylogenetic test for comparing multiple high-dimensional evolutionary rates suggests interplay of evolutionary rates and modularity in lanternfishes (Myctophiformes; Myctophidae). *Evolution*, *69*(9), 2425–2440. https://doi.org/10.1111/evo.12743

Dickson, B. V., Clack, J. A., Smithson, T. R., & Pierce, S. E. (2021). Functional adaptive landscapes predict terrestrial capacity at the origin of limbs. *Nature*, *589*(7841), 242–245. https://doi.org/10.1038/s41586-020-2974-5

Evans, A. R., & Sanson, G. D. (2003). The tooth of perfection: Functional and spatial constraints on mammalian tooth shape. *Biological Journal of the Linnean Society*, *78*(2), 173–191. https://doi.org/10.1046/j.1095-8312.2003.00146.x

Evans, A. R., & Sanson, G. D. (2006). Spatial and functional modeling of carnivore and insectivore molariform teeth. *Journal of Morphology*, *267*(6), 649–662. https://doi.org/10.1002/jmor.10285

Fedorov, A., Beichel, R., Kalpathy-Cramer, J., Finet, J., Fillion-Robin, J.-C., Pujol, S., Bauer, C., Jennings, D., Fennessy, F. M., Sonka, M., Buatti, J., Aylward, S. R., Miller, J. V., Pieper, S., & Kikinis, R. (2012). 3D Slicer as an image computing platform for the quantitative imaging network. *Magnetic Resonance Imaging*, *30*(9), 1323–1341. https://doi.org/10.1016/j.mri.2012.05.001

Fortuny, J., Marcé-Nogué, J., Gil, L., & Galobart, A. (2012). Skull mechanics and the evolutionary patterns of the otic notch closure in capitosaurs (Amphibia: Temnospondyli). *The Anatomical Record*, *295*(7), 1134–1146. https://doi.org/10.1002/ar.22486

Fowler, H. G. (1987). The nest of *Pheidole oxyops* as a pitfall-trap (Hymenoptera: Formicidae). *Pedobiologia*, *30*(5), 373–376. https://doi.org/10.1016/s0031-4056(23)00388-8

Futuyma, D. J., & Moreno, G. (1988). The evolution of ecological specialization. *Annual Review of Ecology and Systematics*, *19*(1), 207–233.

Gil, L., Marcé-Nogué, J., & Sánchez, M. (2015). Insights into the controversy over materials data for the comparison of biomechanical performance in vertebrates. *Palaeontologia Electronica*, *18*(1), 1–24.

Gobin, B., Peeters, C., Billen, J., & Morgan, E. D. (1998). Interspecific trail following and commensalism between the ponerine ant *Gnamptogenys menadensis* and the formicine ant *Polyrhachis rufipes*. *Journal of Insect Behavior*, *11*, 361–369.

Gomes, I. J., Santiago, D. F., Campos, R. I., & Vasconcelos, H. L. (2019). Why do *Pheidole oxyops* (Forel, 1908) ants place feathers around their nests? *Ecological Entomology*, *44*(4), 451–456. https://doi.org/10.1111/een.12722

Gomes, I. J. M. T., Campos, R. I., & Vasconcelos, H. L. (2021). Ecology of *Pheidole oxyops* Forel, 1908, a dominant ant in neotropical

savannas. *Insectes Sociaux*, *68*(1), 69–75. https://doi.org/10.1007/s00040-021-00807-7
Gómez, C., & Espadaler, X. (2013). An update of the world survey of myrmecochorous dispersal distances. *Ecography*, *36*(11), 1193–1201. https://doi.org/10.1111/j.1600-0587.2013.00289.x
Green, P. J., & Hastie, D. I. (2009). Reversible jump MCMC. *Genetics*, *155*(3), 1391–1403.
Hölldobler, B., Braun, U., Gronenberg, W., Kirchner, W. H., & Peeters, C. (1994). Trail communication in the ant *Megaponera foetens* (Fabr.)(Formicidae, Ponerinae). *Journal of Insect Physiology*, *40*(7), 585–593. https://doi.org/10.1016/0022-1910(94)90145-7
Huey, R. B., & Hertz, P. E. (1984). Is a jack-of-all-temperatures a master of none? *Evolution*, *38*(2), 441–444. https://doi.org/10.1111/j.1558-5646.1984.tb00302.x
Irschick, D. J., & Higham, T. E. (2016). *Animal athletes: An ecological and evolutionary approach*. Oxford University Press.
Jansen van Vuuren, L., Kieser, J. A., Dickenson, M., Gordon, K. C., & Fraser-Miller, S. J. (2016). Chemical and mechanical properties of snake fangs. *Journal of Raman Spectroscopy*, *47*(7), 787–795. https://doi.org/10.1002/jrs.4903
Klunk, C. L., Argenta, M. A., Casadei-Ferreira, A., Economo, E. P., & Pie, M. R. (2021). Mandibular morphology, task specialization and bite mechanics in *Pheidole* ants (Hymenoptera: Formicidae). *Journal of the Royal Society Interface*, *18*(179), 20210318. https://doi.org/10.1098/rsif.2021.0318
Klunk, C. L., Argenta, M. A., Rosumek, F. B., Schmelzle, S., van de Kamp, T., Hammel, J. U., Pie, M. R., & Heethoff, M. (2023). Simulated biomechanical performance of morphologically disparate ant mandibles under bite loading. *Scientific Reports*, *13*(1), 16833. https://doi.org/10.1038/s41598-023-43944-8
Krings, W., Marcé-Nogué, J., and Gorb, S. N. (2021). Finite element analysis relating shape, material properties, and dimensions of taenioglossan radular teeth with trophic specializations in Paludomidae (Gastropoda). *Scientific Reports*, *13*(1), 1–15. https://doi.org/10.1038/s41598-021-02102-8
Kugler, C. (1979). Evolution of the sting apparatus in the myrmicine ants. *Evolution*, *33*(1Part1), 117–130. https://doi.org/10.1111/j.1558-5646.1979.tb04668.x
Lachaud, J. P. (1990). Foraging activity and diet in some neotropical ponerine ants. I. *Ectatomma ruidum* Roger (Hymenoptera, Formicidae). *Folia Entomologica Mexicana*, *78*, 241–256.
Li, H., Sun, C. Y., Fang, Y., Carlson, C. M., Xu, H., Ješovnik, A., Sosa-Calvo, J., Zarnowski, R., Bechtel, H. A., Fournelle, J. H., Andes, D. R., Schultz, T. R., Gilbert, P. U. P. A., & Currie, C. R. (2020). Biomineral armor in leafcutter ants. *Nature Communications*, *11*(1), 5792. https://doi.org/10.1038/s41467-020-19566-3
Macalintal, E. A., & Starr, C. K. (1996). Comparative morphology of the stinger in the social wasp genus *Ropalidia* (Hymenoptera: Vespidae). *Memoirs of the Entomological Society of Washington*, *17*, 108–150.
Marcé-Nogué, J. (2020). Mandibular biomechanics as a key factor to understand diet in mammals. In T. Martin, & W. von Koenigswald (Eds.), *Mammalian teeth. Form and function* (pp. 55–80). Verlag Dr. Friedrich Pfeil.
Marcé-Nogué, J., de Esteban-Trivigno, S., Escrig Pérez, C., & Gil Espert, L. (2016). Accounting for differences in element size and homogeneity when comparing finite element models: Armadillos as a case study. *Palaeontologia Electronica*, *19*, 1–22.
Marcé-Nogué, J., De Esteban-Trivigno, S., Püschel, T. A., & Fortuny, J. (2017). The intervals method: A new approach to analyze finite element outputs using multivariate statistics. *PeerJ*, *5*, e3793. https://doi.org/10.7717/peerj.3793
Marcé-Nogué, J., Fortuny, J., Gil, L., & Sánchez, M. (2015). Improving mesh generation in finite element analysis for functional morphology approaches. *Spanish Journal of Palaeontology*, *30*(1), 117–132. https://doi.org/10.7203/sjp.30.1.17227
Marcé-Nogué, J., Püschel, T. A., Daasch, A., & Kaiser, T. M. (2020). Broad-scale morpho-functional traits of the mandible suggest no hard food adaptation in the hominin lineage. *Scientific Reports*, *10*(1), 6793. https://doi.org/10.1038/s41598-020-63739-5
Martins, E. P., & Hansen, T. F. (1996). The statistical analysis of interspecific data: A review and evaluation of phylogenetic comparative methods. *Phylogenies and the Comparative Method in Animal Behavior*, *1*, 22–75.
McPeek, M. A. (2008). The ecological dynamics of clade diversification and community assembly. *The American Naturalist*, *172*(6), E270–E284. https://doi.org/10.1086/593137
Melati, B. G., & Leal, L. C. (2018). Aggressive bodyguards are not always the best: Preferential interaction with more aggressive ant species reduces reproductive success of plant bearing extrafloral nectaries. *PLoS One*, *13*(6), e0199764. https://doi.org/10.1371/journal.pone.0199764
Miao, B. J., Yang, Q. S., Liu, L. Y., & Li, S. W. (2020). The three-cavity microstructures and mechanical properties of honeybee stingers. *Materials Research Express*, *7*(10), 105403. https://doi.org/10.1088/2053-1591/abb96a
Milwich, M., Speck, T., Speck, O., Stegmaier, T., & Planck, H. (2006). Biomimetics and technical textiles: Solving engineering problems with the help of nature's wisdom. *American Journal of Botany*, *93*(10), 1455–1465. https://doi.org/10.3732/ajb.93.10.1455
O'Neill, K. M. (2001). *Solitary wasps: Behavior and natural history*. Cornell University Press.
Packer, L. (2003). Comparative morphology of the skeletal parts of the sting apparatus of bees (Hymenoptera: Apoidea). *Zoological Journal of the Linnean Society*, *138*(1), 1–38. https://doi.org/10.1046/j.1096-3642.2003.00055.x
Pagel, M. (1994). Detecting correlated evolution on phylogenies: A general method for the comparative analysis of discrete characters. *Proceedings of the Royal Society of London, Series B: Biological Sciences*, *255*(1342), 37–45.
Paradis, E., Claude, J., & Strimmer, K. (2004). APE: analyses of phylogenetics and evolution in R language. *Bioinformatics*, *20*(2), 289–290. https://doi.org/10.1093/bioinformatics/btg412
Passos, F. C., & Leal, L. C. (2019). Protein matters: Ants remove herbivores more frequently from extrafloral nectary-bearing plants when habitats are protein poor. *Biological Journal of the Linnean Society*, *127*(2), 407–416. https://doi.org/10.1093/biolinnean/blz033
Paull, J. S., Martin, R. A., & Pfennig, D. W. (2012). Increased competition as a cost of specialization during the evolution of resource polymorphism. *Biological Journal of the Linnean Society*, *107*(4), 845–853. https://doi.org/10.1111/j.1095-8312.2012.01982.x
Pennell, M. W., Eastman, J. M., Slater, G. J., Brown, J. W., Uyeda, J. C., FitzJohn, R. G., Alfaro, M. E., & Harmon, L. J. (2014). Geiger v2. 0: An expanded suite of methods for fitting macroevolutionary models to phylogenetic trees. *Bioinformatics*, *30*(15), 2216–2218. https://doi.org/10.1093/bioinformatics/btu181
Pinheiro, J., Bates, D., R Core Team (2023). Nlme: Linear and Nonlinear Mixed Effects Models. R package version 3.1-164. https://CRAN.R-project.org/package=nlme
Pinheiro, J. C., & Bates, D. M. (2000). Fitting nonlinear mixed-effects models. *Mixed-effects models in S and S-PLUS* (pp. 337–421). Springer.
Pluzhinikov, K. A., Nol'de, D. E., Tertyshnikova, S. M., Sukhanov, S. V., Sobol, A. G., MIu, T., Filippov, A. K., Arsen'ev, A. S., & Grishin, E. V. (1994). Structure-activity study of the basic toxic component of venom from the ant *Ectatomma tuberculatum*. *Bioorganicheskaia Khimiia*, *20*(8–9), 857–871.
Pohl, A., Herrera, S. A., Restrepo, D., Negishi, R., Jung, J. Y., Salinas, C., Wuhrer, R., Yoshino, T., McKittrick, J., Arakaki, A., Nemoto, M., Zavattieri, P., & Kisailus, D. (2020). Radular stylus of *Cryptochiton stelleri*: A multifunctional lightweight and flexible fiber-reinforced composite. *Journal of the Mechanical Behavior of Biomedical Materials*, *111*, 103991. https://doi.org/10.1016/j.jmbbm.2020.103991
Polidori, C. (2011). *Predation in the Hymenoptera: An evolutionary perspective*, Transworld Research Network.
Polly, P. D., Stayton, C. T., Dumont, E. R., Pierce, S. E., Rayfield, E. J., & Angielczyk, K. D. (2016). Combining geometric morphometrics and finite element analysis with evolutionary modeling: Towards

a synthesis. *Journal of Vertebrate Paleontology*, *36*(4), e1111225. https://doi.org/10.1080/02724634.2016.1111225

Price, S. A., Hopkins, S. S., Smith, K. K., & Roth, V. L. (2012). Tempo of trophic evolution and its impact on mammalian diversification. *Proceedings of the National Academy of Sciences of the United States of America*, *109*(18), 7008–7012. https://doi.org/10.1073/pnas.1117133109

Püschel, T. A., Marcé-Nogué, J., Gladman, J. T., Bobe, R., & Sellers, W. I. (2018). Inferring locomotor behaviours in Miocene New World monkeys using finite element analysis, geometric morphometrics and machine-learning classification techniques applied to talar morphology. *Journal of the Royal Society Interface*, *15*(146), 20180520. https://doi.org/10.1098/rsif.2018.0520

Revell, L. J. (2012). Phytools: An R package for phylogenetic comparative biology (and other things). *Methods in Ecology and Evolution*, *3*(2), 217–223. https://doi.org/10.1111/j.2041-210x.2011.00169.x

Revell, L. J., & Collar, D. C. (2009). Phylogenetic analysis of the evolutionary correlation using likelihood. *Evolution*, *63*(4), 1090–1100. https://doi.org/10.1111/j.1558-5646.2009.00616.x

Ribas, C., Oliveira, P., Sobrinho, T., Schoereder, J., & Madureira, M. (2010). The arboreal ant community visiting extrafloral nectaries in the neotropical cerrado savanna. *Terrestrial Arthropod Reviews*, *3*(1), 3–27. https://doi.org/10.1163/187498310x487785

Robertson, P. L. (1968). A morphological and functional study of the venom apparatus in representatives of some major groups of Hymenoptera. *Australian Journal of Zoology*, *16*(1), 133–166. https://doi.org/10.1071/zo9680133

Robinson, S. D., Schendel, V., Schroeder, C. I., Moen, S., Mueller, A., Walker, A. A., McKinnon, N., Neely, G. G., Vetter, I., King, G. F., & Undheim, E. A. (2023). Intra-colony venom diversity contributes to maintaining eusociality in a cooperatively breeding ant. *BMC Biology*, *21*(1), 5. https://doi.org/10.1186/s12915-022-01507-9

Rohlf, F. J., & Corti, M. (2000). Use of two-block partial least-squares to study covariation in shape. *Systematic Biology*, *49*(4), 740–753. https://doi.org/10.1080/106351500750049806

Rohlf, F. J., & Slice, D. (1990). Extensions of the Procrustes method for the optimal superimposition of landmarks. *Systematic Zoology*, *39*(1), 40–59. https://doi.org/10.2307/2992207

Rojas, D., Vale, A., Ferrero, V., & Navarro, L. (2012). The role of frugivory in the diversification of bats in the neotropics. *Journal of Biogeography*, *39*(11), 1948–1960. https://doi.org/10.1111/j.1365-2699.2012.02709.x

Schluter, D. (2000). *The ecology of adaptive radiation*. Oxford University Press.

Serrano-Fochs, S., De Esteban-Trivigno, S., Marcé-Nogué, J., Fortuny, J., & Fariña, R. A. (2015). Finite element analysis of the Cingulata jaw: An ecomorphological approach to armadillo's diets. *PLoS One*, *10*(4), e0120653. https://doi.org/10.1371/journal.pone.0120653

Sharkey, M. J., Carpenter, J. M., Vilhelmsen, L., Heraty, J., Liljeblad, J., Dowling, A. P., Schulmeister, S., Murray, D., Deans, A. R., Ronquist, F., Krogmann, L., & Wheeler, W. C. (2012). Phylogenetic relationships among superfamilies of Hymenoptera. *Cladistics*, *28*(1), 80–112. https://doi.org/10.1111/j.1096-0031.2011.00366.x

Silva, J. R. D., Souza, A. Z. D., Pirovani, C. P., Costa, H., Silva, A., Dias, J. C. T., Delabie, J. H. C., & Fontana, R. (2018). Assessing the proteomic activity of the venom of the ant *Ectatomma tuberculatum* (Hymenoptera: Formicidae: Ectatomminae). *Psyche: A Journal of Entomology*, *1*, 1–11. https://doi.org/10.1155/2018/7915464.

Simpson, G. G. (1953). *The major features of evolution*. Columbia University Press.

Smaers, J. B., & Mongle, C. S. (2018). On the accuracy and theoretical underpinnings of the multiple variance Brownian motion approach for estimating variable rates and inferring ancestral states. *Biological Journal of the Linnean Society*, *121*(1), 229–238. https://doi.org/10.1093/biolinnean/blx003

Smaers, J. B., Mongle, C. S., & Kandler, A. (2016). A multiple variance Brownian motion framework for estimating variable rates and inferring ancestral states. *Biological Journal of the Linnean Society*, *118*(1), 78–94. https://doi.org/10.1111/bij.12765

Snodgrass, R. E. (1933). Morphology of the insect abdomen, Part II, the genital ducts and the ovipositor. *Smithsonian Miscellaneous Collections*, *89*(8), 1–148.

Stayton, C. T. (2019). Performance in three shell functions predicts the phenotypic distribution of hard-shelled turtles. *Evolution*, *73*(4), 720–734. https://doi.org/10.1111/evo.13709

Stroud, J. T., & Losos, J. B. (2016). Ecological opportunity and adaptive radiation. *Annual Review of Ecology, Evolution, and Systematics*, *47*(1), 507–532. https://doi.org/10.1146/annurev-ecolsys-121415-032254

Tamura, K., Stecher, G., & Kumar, S. (2021). MEGA11: Molecular evolutionary genetics analysis version 11. *Molecular Biology and Evolution*, *38*(7), 3022–3027. https://doi.org/10.1093/molbev/msab120

Tamura, K., Tao, Q., & Kumar, S. (2018). Theoretical foundation of the RelTime method for estimating divergence times from variable evolutionary rates. *Molecular Biology and Evolution*, *35*(7), 1770–1782. https://doi.org/10.1093/molbev/msy044

Thomas, M. L., & Framenau, V. W. (2005). Foraging decisions of individual workers vary with colony size in the greenhead ant *Rhytidoponera metallica* (Formicidae, Ectatomminae). *Insectes Sociaux*, *52*(1), 26–30. https://doi.org/10.1007/s00040-004-0768-7

Touchard, A., Koh, J. M., Aili, S. R., Dejean, A., Nicholson, G. M., Orivel, J., & Escoubas, P. (2015). The complexity and structural diversity of ant venom peptidomes is revealed by mass spectrometry profiling. *Rapid communications in Mass Spectrometry*, *29*(5), 385–396. https://doi.org/10.1002/rcm.7116

Uyeda, J. C., & Harmon, L. J. (2014). A novel Bayesian method for inferring and interpreting the dynamics of adaptive landscapes from phylogenetic comparative data. *Systematic Biology*, *63*(6), 902–918. https://doi.org/10.1093/sysbio/syu057

Valenzuela-González, J., López-Méndez, A., & Lachaud, J. P. (1995). Activity patterns and foraging activity in nests of *Ectatomma tuberculatum* (Hymenoptera: Formicidae) in cacao plantations. *Southwestern Entomologist*, *20*(4), 507–515.

Van der Meijden, A., & Kleinteich, T. (2017). A biomechanical view on stinger diversity in scorpions. *Journal of Anatomy*, *230*(4), 497–509. https://doi.org/10.1111/joa.12582

Vincent, J. F. (2002). Arthropod cuticle: A natural composite shell system. *Composites Part A Applied Science and Manufacturing*, *33*(10), 1311–1315. https://doi.org/10.1016/s1359-835x(02)00167-7

Vincent, J. F., & Wegst, U. G. (2004). Design and mechanical properties of insect cuticle. *Arthropod Structure & Development*, *33*(3), 187–199. https://doi.org/10.1016/j.asd.2004.05.006

Walmsley, C. W., Smits, P. D., Quayle, M. R., McCurry, M. R., Richards, H. S., Oldfield, C. C., Wroe, S., Clausen, P. D., & McHenry, C. R. (2013). Why the long face? The mechanics of mandibular symphysis proportions in crocodiles. *PLoS One*, *8*(1), e53873. https://doi.org/10.1371/journal.pone.0053873

Wiens, J. J., Lapoint, R. T., & Whiteman, N. K. (2015). Herbivory increases diversification across insect clades. *Nature Communications*, *6*(1), 8370. https://doi.org/10.1038/ncomms9370

Zhao, L., Ma, J., Wang, T., & Xing, D. (2010). Lightweight design of mechanical structures based on structural bionic methodology. *Journal of Bionic Engineering*, *7*(S4), S224–S231. https://doi.org/10.1016/s1672-6529(09)60239-0

Zhao, Z. L., Zhao, H. P., Ma, G. J., Wu, C. W., Yang, K., & Feng, X. Q. (2015). Structures, properties, and functions of the stings of honeybees and paper wasps: A comparative study. *Biology Open*, *4*(7), 921–928. https://doi.org/10.1242/bio.012195